like domain-containing adhesion molecules. *Genomics* 2006;87:139–50.
11. Williams YN, Masuda M, Sakurai-Yageta M, Maruyama T, Shibuya M, Murakami Y. Cell adhesion and prostate tumor suppressor activity of TSLL2/IGSF4C, an immunoglobulin superfamily molecule homologous to TSLC1/IGSF4. *Oncogene* 2006;25:1446–53.
12. Yageta M, Kuramochi M, Masuda M, Fukami T, Fukuhara H, Maruyama T, Shibuya M, Murakami Y. Direct association of TSLC1 and DAL-1, two distinct tumor suppressor proteins in lung cancer. *Cancer Res* 2002;62:5129–33.
13. Tran YK, Bogler O, Gorse KM, Wieland I, Green MR, Newsham IF. A novel meber of the NF2/ERM/4.1 superfamily with growth suppressing properties in lung cancer. *Cancer Res* 1999;59:35–43.
14. Gutmann DH, Donahoe J, Perry A, Lemke N, Karen G, Kittiniyom K, Rempel AS, Gutierrez AJ, Newsham FI. Loss of DAL-1, a protein 4.1-related tumor suppressor, is an important early event in the pathogenesis of meningiomas. *Hum Mol Genet* 2000;9:1495–500.
15. Kikuchi S, Yamada D, Fukami T, Masuda M, Sakurai-Yageta M, Williams YN, Maruyama T, Asamura H, Matsuno Y, Onizuka M, Murakami Y. Promoter methylation of the DAL-1/4.1B predicts poor prognosis in non-small cell lung cancer. *Clin Cancer Res* 2005;11:2954–61.
16. Kikuchi S, Yamada D, Fukami T, Maruyama T, Ito A, Asamura H, Matsuno Y, Onizuka M, Murakami Y. Hypermethylation of the TSLC1/IGSF4 promoter is associated with tobacco smoking and a poor prognosis in primary non-small cell lung cancer. *Cancer* 2006; 106:1751–8.
17. Heller G, Fong KM, Girard L, Seidl S, End-Pfützenreuter A, Lang G, Gazdar AF, Minna JD, Zielinski CC, Zöchbauer-Müller S. Expression and methylation pattern of TSLC1 cascade genes in lung carcinomas. *Oncogene* 2006;25:959–68.
18. Heller G, Geradts J, Ziegler B, Newsham I, Filipits M, Markis-Ritzinger EM, Kandioler D, Berger W, Stiglbauer W, Depisch D, Pirker R, Zielinski CC, et al. Downregulation of TSLC1 and DAL-1 expression occurs frequently in breast cancer. *Breast Cancer Res Treat* 2007;103: 283–91.
19. Lusis E, Gutmann DH. Meningioma: an update. *Curr Opin Neurol* 2004;17:687–92.
20. Ramez M, Blot-Chabaud M, Cluzeaud F, Chanan S, Patterson M, Walensky LD, Marfatia S, Baines AJ, Chasis JA, Conboy JG, Mohandas N, Gascard P. Distinct distribution of specific members of protein 4.1 gene family in the mouse nephron. *Kidney Int* 2003;63:1321–37.
21. Yamada D, Kikuchi S, Williams YN, Sakurai-Yageta M, Masuda M, Maruyama T, Tomita K, Gutmann DH, Kakizoe T, Kitamura T, Murakami Y. Promoter hypermethylation of the potential tumor suppressor DAL-1/4.1B gene in renal clear cell carcinoma. *Int J Cancer* 2006;118: 916–23.
22. Sakurai-Yageta M, Masuda M, Tsuboi Y, Ito A, Murakami Y. Tumor suppressor CADM1 is involved in epithelial cell structure. *Biochem Biophys Res Commun* 2009;90:977–82.
23. Koma Y, Furuno T, Hagiyama M, Hamaguchi K, Nakanishi M, Masuda M, Hirota S, Yokozaki H, Ito A. Cell adhesion molecule 1 is a novel pancreatic-islet cell adhesion molecule that mediates nerve-islet cell interactions. *Gastroenterology* 2008;134: 1544–54.
24. Veigl ML, Kasturi L, Olechnowicz J, Ma AH, Lutterbaugh JD, Periyasamy S, Li GM, Drummond J, Modrich PL, Sedwick WD, Markowitz SD. Bialleic inactivation of hMLH1 by epigenetic gene silencing, a novel mechanism causing human MSI cancers. *Proc Natl Acad Sci USA* 1998;95: 8698–702.
25. Zhou Y, Du G, Hu X, Yu S, Liu Y, Xu Y, Huang X, Liu J, Yin B, Fan M, Peng X, Qiang B, et al. Nectin-like molecule 1 is a protein 4.1N associated protein and recruits protein 4.1N from cytoplasm to the plasma membrane. *Biochim Biophys Acta* 2005;1669:142–54.
26. Nickerson ML, Jaeger E, Shi Y, Durocher JA, Mahurkar S, Zaridze D, Matveev V, Janout V, Kollarova H, Bencko V, Navratilova M, Szeszenia-Dabrowska N, et al. Improved identification of von Hippel-Lindau gene alterations in clear cell renal tumors. *Clin Cancer Res* 2008;14: 4726–34.
27. Dall'Oglio MF, Antunes AA, Sarkis AS, Crippa A, Leite KR, Lucon AM, Srougi M. Microvascular tumour invasion in renal cell carcinoma: the most important prognostic factor. *BJ U Int* 2007;100:552–5.
28. Strewler GJ, Wronski TJ, Halloran BP, Miller SC, Leung SC, Williams RD, Nissenson RA. Pathogenesis of hypercalcemia in nude mice bearing a human renal carcinoma. *Endocrinology* 1986;119:303–10.
29. Dreijerink K, Braga E, Kuzmin I, Geil L, Duh FM, Angeloni D, Zbar B, Lerman MI, Stanbridge EJ, Minna JD, Protopopov A, Li J, et al. The candidate tumor suppressor gene, RASSF1A, from human chromosome 3p21.3 is involved in kidney tumorigenesis. *Proc Natl Acad Sci USA* 2001;98:7504–9.
30. Morrissey C, Martinez A, Zatyka M, Agathanggelou A, Honorio S, Astuti D, Morgan NV, Moch H, Richards FM, Kishida T, Yao M, Schraml P, et al. Epigenetic inactivation of the RASSF1A 3p21.3 tumor suppressor gene in both clear cell and papillary renal cell carcinoma. *Cancer Res* 2001;61:7277–81.
31. Dulaimi E, Caceres II, Uzzo RG, Al-Saleem T, Greenberg RE, Polascik TJ, Babb JS, Grizzle WE, Cairns P. Promoter hypermethylation profile of kidney cancer. *Clin Cancer Res* 2004;10:3972–9.
32. Murakami Y. Involvement of a cell adhesion molecule, TSLC1/IGSF4, in human oncogenesis. *Cancer Sci* 2005;96: 543–52.
33. Curto M, Cole BK, Lallemand D, Liu CH, McClatchey AI. Contact-dependent inhibition of EGFR signaling by Nf2/Merlin. *J Cell Biol* 2007;177:893–903.
34. Kunitz A, Wolter M, van den Boom J, Felsberg J, Tews B, Hahn M, Benner A, Sabel M, Lichter P, Reifenberger G, von Deimling A, Hartmann C. DNA hypermethylation and aberrant expression of the EMP3 gene at 19q13.3 in human gliomas. *Brain Pathol* 2007;17:363–70.
35. Tews B, Felsberg J, Hartmann C, Kunitz A, Hahn M, Toedt G, Neben K, Hummerich L, von Deimling A, Reifenberger G, Lichter P. Identification of novel oligodendroglioma-associated candidate tumor suppressor genes in 1p36 and 19q13 using microarray-based expression profiling. *Int J Cancer* 2006;119: 792–800.
36. Morris ZS, McClatchey A. Aberrant epithelial morphology and persistent epidermal growth factor receptor signaling in a mouse model of renal carcinoma. *Proc Natl Acad Sci USA* 2009;106:9767–72.
37. Sun CX, Robb VA, Gutmann DH. Protein 4.1 tumor suppressors: getting a FERM grip on growth regulation. *J Cell Sci* 2002; 115:3991–4000.
38. Kawano S, Ikeda W, Kishimoto M, Ogita H, Takai Y. Silencing of ErbB3/ErbB2 signaling by immunoglobulin-like Necl-2. *J Biol Chem* 2009;284:23793–805.
39. Doherty P, Walsh FS. CAM-FGF receptor interactions: a model for axonal growth. *Mol Cell Neurosci* 1996;8:99–111.
40. Surace EI, Lusis E, Murakami Y, Scheithauer BW, Perry A, Gutmann DH. Loss of tumor suppressor in lung cancer-1 (TSLC1) expression in meningioma correlates with increased malignancy grade and reduced patient survival. *J Neuropathol Exp Neurol* 2004;63:1015–27.

Int J Hematol
DOI 10.1007/s12185-013-1314-z

CASE REPORT

Development of peripheral T-cell lymphoma not otherwise specified in an HTLV-1 carrier

Tomohiro Ishigaki · Masamichi Isobe · Seiichiro Kobayashi · Koichiro Yuji · Nobuhiro Ohno · Nobukazu Watanabe · Arinobu Tojo · Kaoru Uchimaru

Received: 2 October 2012 / Revised: 12 March 2013 / Accepted: 13 March 2013

Abstract Human T-cell leukemia virus type 1 (HTLV-1) causes adult T-cell leukemia (ATL) after a long latency period of about 60 years. As the mature T-cell neoplasms that emerge in patients infected with HTLV-1 are often ATL, T-cell neoplasms developing in such patients tend to be diagnosed simply as ATL without further investigation. However, not all T-cell neoplasms that develop in HTLV-1-infected cases are ATL. Mature T-cell malignancies other than ATL should be carefully excluded in patients infected with HTLV-1, as these sometimes closely resemble ATL in their clinical, morphological, and histological features. Here, we present a case of peripheral T-cell lymphoma not otherwise specified (PTCL-NOS) in an HTLV-1 carrier. Confirmation of monoclonal integration of the virus with Southern blotting leads to a definite diagnosis of ATL. Although we did not detect the monoclonal integration band of HTLV-1 in this case, the high HTLV-1 proviral load complicated the diagnosis. Multicolor flow cytometric analysis clearly showed that HTLV-1 was not integrated in the tumor cells, and facilitated discrimination of PTCL-NOS from ATL.

Keywords Human T-cell leukemia virus type 1 (HTLV-1) · Adult T-cell leukemia (ATL) · Multicolor flow cytometry · Peripheral T-cell lymphoma not otherwise specified (PTCL-NOS)

Introduction

Human T-cell leukemia virus type 1 (HTLV-1) is an etiological agent of adult T-cell leukemia (ATL) [1, 2], which is one of the mature T-cell neoplasms. According to the Shimoyama criteria [3], four clinical subtypes of ATL exist: smoldering, chronic, lymphoma, and acute. The former two are considered indolent ATL, and the others are aggressive ATL. Patients with aggressive- or chronic-type ATL with unfavorable prognostic factors are subjected to combination chemotherapy, whereas patients with smoldering type or chronic type ATL without unfavorable prognostic factors are observed initially without therapy, because conventional chemotherapy does not improve overall survival [4].

This disease has a long latency period of about 60 years from HTLV-1 infection, and the cumulative incidence of ATL is estimated to be only 5 % among HTLV-1 carriers. Despite such a low incidence, mature T-cell neoplasms that emerge in patients infected with HTLV-1 are usually ATL. Therefore, mature T-cell neoplasms in patients infected with HTLV-1 tend to be diagnosed as ATL without further investigation. However, T-cell neoplasms occurring in such cases are not always ATL, and rare cases of T-cell neoplasms other than ATL developing in HTLV-1 carriers have been reported [5–7]. The definitive diagnosis of ATL

T. Ishigaki (✉) · M. Isobe · K. Yuji · N. Ohno · A. Tojo · K. Uchimaru
Department of Hematology and Oncology, Research Hospital, The Institute of Medical Science, The University of Tokyo, 4-6-1 Shirokanedai, Minato-ku, Tokyo 108-8639, Japan
e-mail: ishigaki@ims.u-tokyo.ac.jp

T. Ishigaki · N. Watanabe
Laboratory of Diagnostic Medicine, Division of Stem Cell Therapy, The Institute of Medical Science, The University of Tokyo, 4-6-1 Shirokanedai, Minato-ku, Tokyo 108-8639, Japan

S. Kobayashi · A. Tojo
Division of Molecular Therapy, The Institute of Medical Science, The University of Tokyo, 4-6-1 Shirokanedai, Minato-ku, Tokyo 108-8639, Japan

Published online: 09 April 2013

requires not only verification of HTLV-1 infection, but also confirmation of monoclonal integration of the virus by laboratory testing such as Southern blotting. However, the discrimination of ATL and other T-cell malignancies with typical ATL clinical features is sometimes difficult.

Here we present a case of peripheral T-cell lymphoma, not otherwise specified (PTCL-NOS), which we definitively discriminated from ATL in an HTLV-1 infected case with a high proviral load.

Case report

Abdominal ultrasonography revealed a hypoechoic mass in the liver of a 65-year-old woman for the first time in July 2008. Further examinations revealed that the patient was seropositive for the anti-HTLV-1 antibody. White blood cell count was 13.1 $\times$ 10^9/L, and abnormal lymphocytes were seen in peripheral blood, which accounted for 36 % of the white blood cells. A physical examination revealed a swollen left inguinal lymph node, and a lymphadenectomy elucidated mature T-cell lymphoma. No other lymph nodes were palpable, and gallium scintigraphy showed no abnormal accumulation. She was diagnosed with chronic-type ATL, which was later found to be incorrect, without confirmation of monoclonal proliferation of HTLV-1 infected cells by Southern blotting. As she had no unfavorable prognostic factors such as low serum albumin, high lactate dehydrogenase (LDH), and high blood urea nitrogen concentrations, she had been under close observation, without progression of lymphadenopathy, elevation of LDH, or an increase in white blood cells for about 1 year. In October 2009, swelling of the upper hard palatine, and cervical lymphadenopathy appeared. Abnormal lymphocytes in peripheral blood increased at the same time. She was referred to our hospital in November 2009.

A physical examination revealed generalized lymphadenopathy, hepatosplenomegaly, and a 1.8-cm mass accompanying central ulceration in the upper hard palatine. Laboratory data were as follows: white blood cells, 14.8 $\times$ 10^9/L with 28 % abnormal lymphocytes; LDH, 264 IU/L; soluble interleukin-2 receptor (sIL2R), 1630 U/ml; and HTLV-1 proviral load, 23.7 copies/100 mononuclear cells.

Large and small morphologically abnormal lymphocytes, which have a basophilic cytoplasm, irregularly shaped nuclei, relatively coarse chromatin, and prominent nucleoli, were seen in peripheral blood (Fig. 1a). Some of these cells contained nuclear abnormalities such as notching, indentation, convolution, and lobulation. While they were similar in appearance to cells that are often seen in

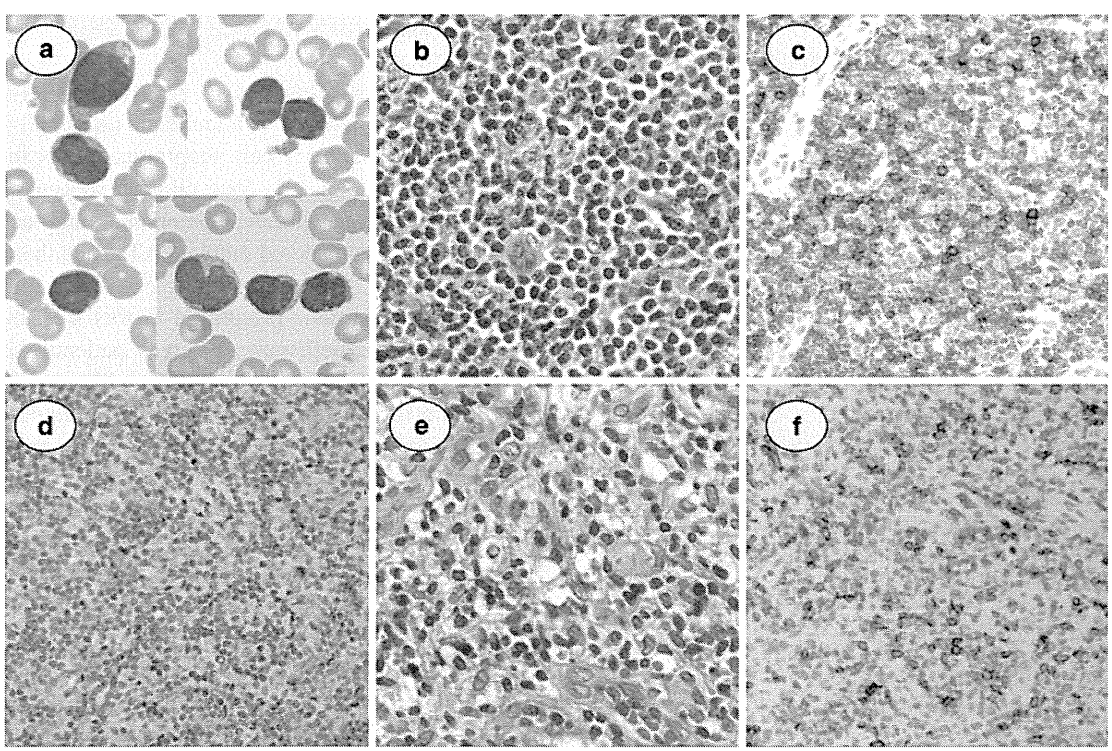

Fig. 1 Abnormal lymphocytes were seen in peripheral blood (**a** Wright-Giemsa staining), and invaded the inguinal lymph node (**b** HE staining; **c** anti-CD8 staining; **d** anti-CD4 staining) and hard palatine (**e** HE staining; **f** anti-CD8 staining). In immunohistochemical staining, positive cells are shown in *brown*

ATL, typical flower cells were not observed. Almost all of the morphologically abnormal lymphocytes were confirmed to be phenotypically abnormal T cells, which were negative for CD7, despite CD2, CD3, and CD5 positivity. Although some were CD4 positive, the others were negative, and about half of the CD4 negative lymphocytes expressed CD8 faintly. A review of previous inguinal lymph node biopsy specimens showed that lymphoid follicles were destroyed and invaded by a diffuse proliferation of abnormal lymphocytes (Fig. 1b) that lost CD7 expression. As seen in the peripheral blood, small-to-large-sized abnormal lymphocytes were admixed in the biopsies. Most of the abnormal lymphocytes were positive for CD3, lacked CD4, and about half expressed CD8 faintly (Fig. 1c, d). In addition, we performed a biopsy from the hard palatine tumor. Abnormal lymphocytes, the majority of which were CD4 negative and similar to cells seen in the lymph node specimen, occupied the tumor (Fig. 1e, f). Hence, these CD4-negative cells were considered tumor cells.

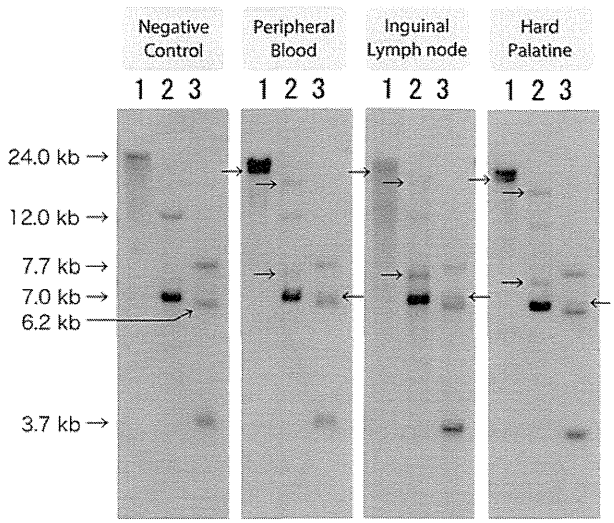

Fig. 2 Analysis of T-cell receptor Cβ1 gene rearrangements by Southern blotting after digestion with *Bam*HI (*1*), *Eco*RV (*2*), and *Hin*dIII (*3*). The same monoclonal T-cell receptor rearrangement bands were observed in all peripheral blood, inguinal lymph node, and hard palatine samples

T-cell receptor rearrangement assays indicated the same clonal T-cell receptor Cβ1 gene rearrangements in all peripheral blood, inguinal lymph node, and hard palatine samples (Fig. 2). In contrast, evaluation of HTLV-1 integration by Southern blot analysis showed a polyclonal smear pattern in peripheral blood but was negative in the inguinal lymph node and the hard palatine (Fig. 3). These results suggest that the swollen lymph nodes and hard palatine were not caused by ATL. Consequently, her diagnosis was changed to PTCL-NOS in an asymptomatic HTLV-1 carrier, and chronic-type ATL was excluded.

The patient received chemotherapy consisting of six courses of the CHOP (cyclophosphamide, doxorubicin, vincristine, and prednisone) regimen and went into complete remission. However, she relapsed after 1 month, and abnormal lymphocytes in the peripheral blood increased abruptly. Because she had a high HTLV-1 proviral load in the peripheral blood, we analyzed these abnormal lymphocytes by multicolor flow cytometry to confirm the diagnosis of PTCL-NOS and to exclude CD8-positive ATL (Fig. 4). Peripheral blood T-cells were classified into four groups: CD4+/CD8−, CD4−/CD8+, CD4−/CD8−, and CD4−/CD8dim. Based on the pathological results, the latter two groups of T-cells were considered to be counterparts of tumor cells in the hard palatine. We collected cells in each fraction by cell sorting and assessed HTLV-1 proviral load using real-time polymerase chain reaction

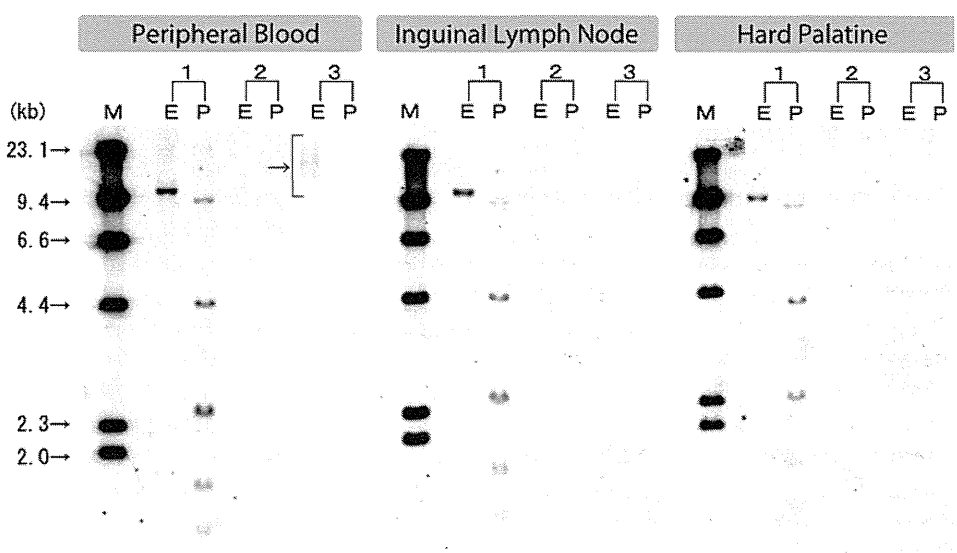

Fig. 3 Analysis of human T-cell leukemia virus type 1 (HTLV-1) proviral integration by Southern blotting after digestion with *Eco*RI (*E*) and *Pst*I (*P*). Samples (*lane 3*), molecular weight marker (*lane M*), positive control (*lane 1*), and negative control (*lane 2*). A peripheral blood sample showed a polyclonal smear pattern, but samples from an inguinal lymph node and the hard palatine were negative

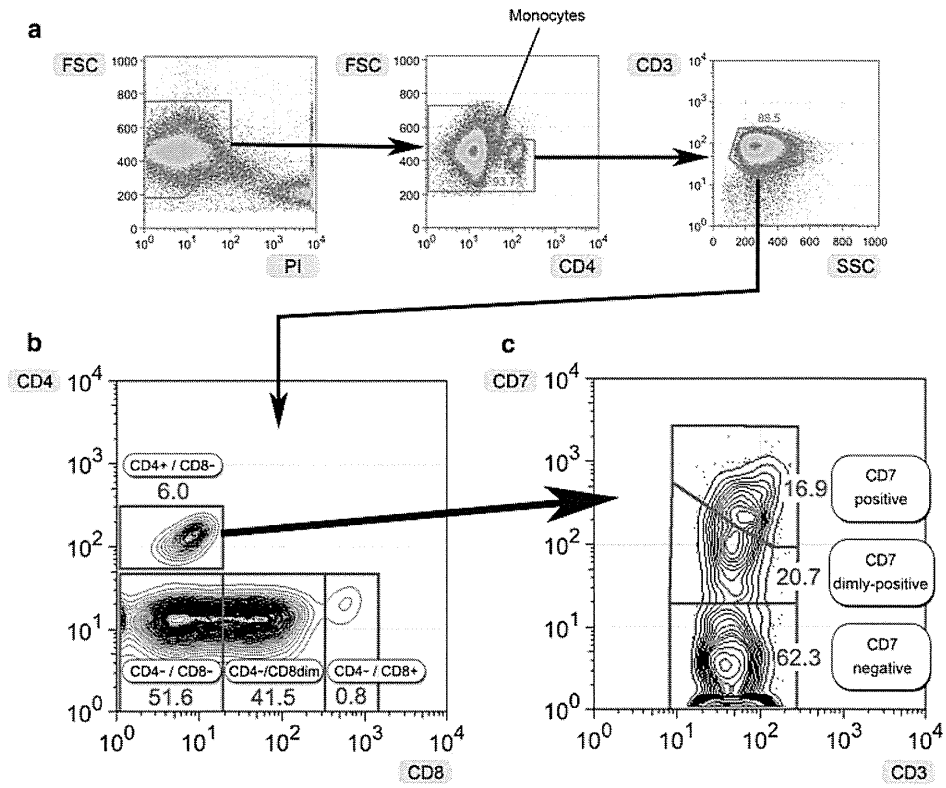

Fig. 4 Multicolor flow cytometric analysis and sorting at the first relapse. **a** Panels **b** and **c** were constructed based on the gating procedure shown here. Dead cells and monocytes were eliminated sequentially, and CD3-positive cells were gated. **b** A CD4 vs. CD8 plot of live T cells was constructed, and was able to separate CD4+/CD8−, CD4−/CD8+, CD4−/CD8−, and CD4−/CD8dim cells. **c** CD4+ cells in **b** were plotted on a CD3 vs. CD7 plot

(PCR). The proviral loads of CD4+/CD8−, CD4−/CD8−, and CD4−/CD8dim were 129.1, 0.2, and 0.0 copies/100 cells, respectively. These data indicate that HTLV-1 infected cells were CD4 positive. We confirmed again that the patient had PTCL-NOS and polyclonal CD4-positive HTLV-1 infected cells. These results showed that she was an HTLV-1 asymptomatic carrier. Subsequent chemotherapy, including two courses of ESHAP (etoposide, methylprednisolone, cytarabine, and cisplatin) and four courses of low-dose VP16, was administered. She went into a second complete remission but relapsed again.

Materials and methods

Multicolor flow cytometry and cell sorting

Peripheral blood mononuclear cells (PBMCs) were isolated from whole blood by density gradient centrifugation using Lymphoprep (Axis-Shield, Dundee, UK) and suspended in phosphate-buffered saline containing 3 % mouse serum (DAKO, Glostrup, Denmark) to prevent non-specific antibody binding. The cells were stained using a combination of phycoerythrin (PE)-CD7 (BD Biosciences, San Jose, CA, USA), APC-Cy7-CD3 (BD PharMingen, San Jose, CA, USA), Pacific Blue-CD8 (Caltag, Paisley, UK), and Pacific Orange-CD4 (Caltag). Propidium iodide (Sigma, St Louis, MO, USA) was added to stain dead cells immediately prior to the flow cytometry analysis. A BD FACS Aria II instrument (BD Immunocytometry Systems, San Jose, CA, USA) was used to analyze and sort the cells. Appropriate isotypes were used as negative controls. Data were analyzed using the FlowJo software, version 9.5.2 (Treestar, San Carlos, CA, USA). The borderlines in Fig. 4 were drawn according to the contour lines and negative controls.

Proviral load

HTLV-1 proviral load was determined by real-time quantitative PCR (TaqMan method) using the ABI Prism 7000 Sequence Detection System (Applied Biosystems, Foster City, CA, USA), as described previously [8]. In brief, genomic DNA was extracted from PBMCs and amplified using the HTLV-1 pX region-specific primer pair at 0.1 μM (forward primer 5′-CGGATACCCAGTCTACGTGTT-3′ and reverse primer 5′-CAGTAGGGCGTGACGATGT A-3′), FAM-labeled probe at 0.1 μM (5′-CTGTGTAC AAGGCGACTGGTGCC-3′), and 1× TaqMan Universal PCR Master Mix (Applied Biosystems). The PCR mixture was subjected to 50 cycles of denaturation (95 °C, 15 s) and annealing to extension (60 °C, 1 min) after initial *Taq* polymerase activation (95 °C, 10 min). The RNase P Control Reagent (Applied Biosystems) was used as an internal control to calculate input cell number. DNA extracted from

TL-Om1, an ATL-derived cell line, and normal human PBMCs were adopted as positive and negative controls, respectively. The HTLV-1 proviral load (copies/100 cells) was calculated as the copy number of the pX region per input cell number. The TL-Om1 values were adjusted to 100 % to correct for the deviation in the acquired values, and the sample values were corrected by proportional calculation.

Discussion

Here, we present a case of PTCL-NOS in a patient infected with HTLV-1. Although T-cell neoplasms developing in patients infected with HTLV-1 tend simply to be diagnosed as ATL, they occasionally lead to an incorrect diagnosis. Indeed, our results show that the patient described in this case was initially misdiagnosed as chronic-type ATL. These findings demonstrate that obtaining a correct diagnosis may be difficult without performing Southern blotting because this case was similar to ATL clinically, morphologically, and histologically.

This case had many features in common with ATL. The clinical manifestations of generalized lymphadenopathy and hepatosplenomegaly were consistent with ATL. High HTLV-1 proviral load and the emergence of abnormal lymphocytes in peripheral blood are more likely to occur in ATL. The pathological findings were indistinguishable from those of ATL. The histological features of ATL are generally a diffuse proliferation of abnormal lymphoid cells that vary in size and shape [8], and the pleomorphic pattern seen in the lymph node and hard palatine of this patient was also compatible with ATL. ATL is characterized by a wide variety of pathological features [9], making its pathological diagnosis or exclusion more difficult.

However, several findings were incompatible with ATL in this case. First, ATL often accompanies considerably high sIL2R. Mean sIL2R levels of lymphoma and acute subtypes are reported to be 34,620 and 45,940 U/ml, respectively [10], whereas the sIL2R level in this case was very low, despite generalized lymphadenopathy and hepatosplenomegaly. Second, tumor cells in this case were negative for CD4 and dimly positive for CD8, although CD8 expression did not rule out ATL. Confirmation of monoclonal integration of HTLV-1 provirus is necessary for a diagnosis of ATL. In this case, examination of monoclonal HTLV-1 integration by Southern blotting was negative in the peripheral blood, an inguinal lymph node, and the hard palatine.

One of the characteristic features of this case was the high HTLV-1 proviral load in peripheral blood, which made the diagnosis confusing. We have reported that CD4+ cells in patients infected with HTLV-1 can be classified into three groups: CD7-positive (CD7P), CD7-dimly positive (CD7D), and CD7-negative (CD7N) using multicolor flow cytometry [11]. We have also investigated the proportion of CD7D and CD7N populations in HTLV-1 carriers and patients with indolent ATL. The analyses revealed that the proportion of CD7D and CD7N in CD4+ cells became higher with progression to ATL, and a proportion of CD7P < 55 % was a high-risk factor for developing ATL [12]. As indicated in Fig. 4, the CD7P population accounted for 16.9 % in this case; therefore, this patient was estimated to be a high-risk carrier with a high HTLV-1 proviral load in peripheral blood. Flow cytometric sorting clearly showed that HTLV-1 was not integrated in dimly CD8-positive or CD8-negative tumor cells (Fig. 4), which again excluded ATL.

Table 1 Previous reports of HTLV-1 carriers with T-cell neoplasms other than ATL

Diagnosis	Patient	First diagnosis (corrected later)	HTLV-1 infection	HTLV-1 monoclonal integration	Phenotype (main pathologic lesions)	Reference
T-cell granular lymphocyte (T-LGL) leukemia	60 years old male		Seropositive	Confirmed negative	CD2+ CD3+ CD4− CD5+ CD7+ CD8+ CD16− CD20dim CD25− CD56+ (PB: peripheral blood)	[5]
Primary cutaneous CD8+ aggressive epidermotropic cytotoxic T-cell lymphoma	58 years old female	Smouldering type of ATL	Seropositive	Confirmed negative	CD3+ CD4− CD5− CD7+ CD8+ CD20− CD25− granzyme B+ (Skin)	[6]
Angioimmunoblastic T-cell lymphoma (AITL)	82 years old female		Seropositive	Confirmed negative	CD2+ CD3+ CD4+ CD5+ CD7+ (down-regulated) CD8− CD20− CD25− granzyme B− (LN: lymph node)	[7]
Peripheral T-cell lymphoma not otherwise specified (PTCL-NOS)	65 years old female	Chronic type of ATL	Seropositive	Confirmed negative	CD2+ CD3+ CD4− CD5+ CD7− CD8−/dim CD20− CD25− (PB, LN and hard palatine)	This report, 2013

Some reports have suggested that HTLV-1 infection is associated with an increased risk of malignancies other than ATL [13, 14]. Patients with B-cell lymphoma and HTLV-1 infection have been reported, and it is known that they have a poorer prognosis than those without HTLV-1 infection, probably because HTLV-1 reduces the number of cytotoxic T cells [15]. The HTLV-1 basic leucine zipper factor contributes to impaired cellular immunity by suppressing Th1 cytokine production [16]. Taking these reports into consideration, HTLV-1 infection may have affected the aggressive course of PTCL-NOS in this case.

Only rare cases of T-cell neoplasms other than ATL have been reported in HTLV-1 infected patients. This may be due to the low incidence of T-cell neoplasms other than ATL, compared to ATL. However, some may be misdiagnosed as ATL due to difficulties in discriminating the various neoplasms. As shown in Table 1, T-cell granular lymphocyte (T-LGL) leukemia [5], primary cutaneous CD8+ aggressive epidermotropic cytotoxic T-cell lymphoma [6], and angioimmunoblastic T-cell lymphoma (AILT) [7] were previously reported with verification of the lack of HTLV-1 integration. In addition, Hodgkin's lymphoma (HL) and anaplastic large cell lymphoma (ALCL) in HTLV-1 carriers were briefly reported [17]. These results are similar to our findings in that some patients were initially diagnosed with ATL. Primary brain T-cell lymphoma has also been reported repeatedly, but the absence of HTLV-1 integration in lymphoma cells has not been evaluated [18].

In summary, we report a case of PTCL-NOS in a patient with HTLV-1 infection. Mature T-cell neoplasms other than ATL should be carefully excluded in patients infected with HTLV-1. In addition, multicolor flow cytometry, which showed clearly that HTLV-1 was not integrated in tumor cells, was helpful for differential diagnosis from ATL.

Conflict of interest The authors declare no conflicts of interest.

References

1. Matsumoto M, Nomura K. Clinical and hematological features of adult T cell leukemia in southern part of Kyushu, Japan (author's transl). Rinsho Ketsueki. 1979;20:1040–7.
2. Yoshida M, Miyoshi I, Hinuma Y. Isolation and characterization of retrovirus from cell lines of human adult T-cell leukemia and its implication in the disease. Proc Natl Acad Sci USA. 1982;79:2031–5.
3. Shimoyama M. Diagnostic criteria and classification of clinical subtypes of adult T-cell leukaemia-lymphoma. A report from the Lymphoma Study Group (1984–87). Br J Haematol. 1991;79:428–37.
4. Ishitsuka K, Tamura K. Treatment of adult T-cell leukemia/lymphoma: past, present, and future. Eur J Haematol. 2008;80:185–96.
5. Nakano-Akamatsu S, Takahashi R, Sekioka Y, et al. CD20- and CD56-positive T-cell large granular lymphocyte leukemia in a human T-cell leukemia virus type 1 carrier. Int J Hematol. 2007;86:348–51.
6. Ohmatsu H, Sugaya M, Fujita H, et al. Primary cutaneous CD8+ aggressive epidermotropic cytotoxic T-cell lymphoma in a human T-cell leukaemia virus type-1 carrier. Acta Derm Venereol. 2010;90:324–5.
7. Chuang SS, Ichinohasama R, Chu JS, et al. Differential diagnosis of angioimmunoblastic T-cell lymphoma with seropositivity for anti-HTLV antibody from adult T-cell leukemia/lymphoma. Int J Hematol. 2010;91:687–91.
8. Iwanaga M, Watanabe T, Utsunomiya A, et al. Human T-cell leukemia virus type I (HTLV-1) proviral load and disease progression in asymptomatic HTLV-1 carriers: a nationwide prospective study in Japan. Blood. 2010;116:1211–9.
9. Ohshima K. Pathological features of diseases associated with human T-cell leukemia virus type I. Cancer Sci. 2007;98:772–8.
10. Kamihira S, Atogami S, Sohda H, et al. Significance of soluble interleukin-2 receptor levels for evaluation of the progression of adult T-cell leukemia. Cancer. 1994;73:2753–8.
11. Tian Y, Kobayashi S, Ohno N, et al. Leukemic T cells are specifically enriched in a unique CD3(dim) CD7(low) subpopulation of CD4(+) T cells in acute-type adult T-cell leukemia. Cancer Sci. 2011;102:569–77.
12. Kobayashi S, Tian Y, Ohno N, et al. The CD3 versus CD7 plot in multicolor flow cytometry reflects progression of disease stage in patients infected with HTLV-I. PLoS ONE. 2013;8:e53728.
13. Asou N, Kumagai T, Uekihara S, et al. HTLV-I seroprevalence in patients with malignancy. Cancer. 1986;58:903–7.
14. Kozuru M, Uike N, Muta K, et al. High occurrence of primary malignant neoplasms in patients with adult T-cell leukemia/lymphoma, their siblings, and their mothers. Cancer. 1996;78:1119–24.
15. Suefuji H, Ohshima K, Hayabuchi N, et al. HTLV-1 carriers with B-cell lymphoma of localized stage head and neck: prognosis, clinical and immunopathological features. Br J Haematol. 2003;123:606–12.
16. Sugata K, Satou Y, Yasunaga JI, et al. HTLV-1 bZIP factor impairs cell-mediated immunity by suppressing production of Th1 cytokines. Blood. 2012;119(2):434–44.
17. Imaizumi Y, Tsukasaki K, Tsushima H, et al. Lymphoma cases without detectable monoclonal HTLV-1 integration in HTLV-1 carrier. Rinsho Ketsueki. 2012;53:1359.
18. Lotan I, Khlebtovsky A, Inbar E, et al. Primary brain T-cell lymphoma in an HTLV-1 serologically positive male. J Neurol Sci. 2012;314:163–5.

OPEN ACCESS Freely available online

PLOS ONE

The CD3 versus CD7 Plot in Multicolor Flow Cytometry Reflects Progression of Disease Stage in Patients Infected with HTLV-I

Seiichiro Kobayashi[1], Yamin Tian[1,2], Nobuhiro Ohno[3], Koichiro Yuji[3], Tomohiro Ishigaki[4], Masamichi Isobe[3], Mayuko Tsuda[3], Naoki Oyaizu[5], Eri Watanabe[4], Nobukazu Watanabe[4], Kenzaburo Tani[2], Arinobu Tojo[1,3], Kaoru Uchimaru[3]*

1 Division of Molecular Therapy, Institute of Medical Science, The University of Tokyo, Tokyo, Japan, **2** Department of Molecular Genetics, Medical Institute of Bioregulation, Kyushu University, Fukuoka, Japan, **3** Department of Hematology/Oncology, Research Hospital, Institute of Medical Science, The University of Tokyo, Tokyo, Japan, **4** Laboratory of Diagnostic Medicine, Division of Stem Cell Therapy, Institute of Medical Science, The University of Tokyo, Tokyo, Japan, **5** Clinical Laboratory, Research Hospital, Institute of Medical Science, The University of Tokyo, Tokyo, Japan

Abstract

Purpose: In a recent study to purify adult T-cell leukemia-lymphoma (ATL) cells from acute-type patients by flow cytometry, three subpopulations were observed in a CD3 versus CD7 plot (H: $CD3^{high}CD7^{high}$; D: $CD3^{dim}CD7^{dim}$; L: $CD3^{dim}CD7^{low}$). The majority of leukemia cells were enriched in the L subpopulation and the same clone was included in the D and L subpopulations, suggesting clonal evolution. In this study, we analyzed patients with indolent-type ATL and human T-cell leukemia virus type I (HTLV-I) asymptomatic carriers (ACs) to see whether the CD3 versus CD7 profile reflected progression in the properties of HTLV-I-infected cells.

Experimental Design: Using peripheral blood mononuclear cells from patient samples, we performed multi-color flow cytometry. Cells that underwent fluorescence-activated cell sorting were subjected to molecular analyses, including inverse long PCR.

Results: In the D(%) versus L(%) plot, patient data could largely be categorized into three groups (Group 1: AC; Group 2: smoldering- and chronic-type ATL; and Group 3: acute-type ATL). Some exceptions, however, were noted (*e.g.*, ACs in Group 2). In the follow-up of some patients, clinical disease progression correlated well with the CD3 versus CD7 profile. In clonality analysis, we clearly detected a major clone in the D and L subpopulations in ATL cases and, intriguingly, in some ACs in Group 2.

Conclusion: We propose that the CD3 versus CD7 plot reflects progression of disease stage in patients infected with HTLV-I. The CD3 versus CD7 profile will be a new indicator, along with high proviral load, for HTLV-I ACs in forecasting disease progression.

Citation: Kobayashi S, Tian Y, Ohno N, Yuji K, Ishigaki T, et al. (2013) The CD3 versus CD7 Plot in Multicolor Flow Cytometry Reflects Progression of Disease Stage in Patients Infected with HTLV-I. PLoS ONE 8(1): e53728. doi:10.1371/journal.pone.0053728

Editor: Jean-Pierre Vartanian, Institut Pasteur, France

Received August 31, 2012; **Accepted** December 4, 2012; **Published** January 22, 2013

Funding: This study was supported by the Ministry of Education, Culture, Sports, Science and Technology, Japan. The funders had no role in study design, data collection and analysis, decision to publish, or preparation of the manuscript.

Competing Interests: The authors have declared that no competing interests exist.

* E-mail: uchimaru@ims.u-tokyo.ac.jp

Introduction

Human T-cell leukemia virus type I (HTLV-I) is the agent that causes HTLV-I-associated diseases, such as adult T-cell leukemia-lymphoma (ATL), HTLV-I-associated myelopathy/tropical spastic paraparesis (HAM/TSP), and HTLV-I uveitis (HU) [1–3]. Approximately 10–20 million people are infected with the HTLV-I virus worldwide [4]. The lifetime risk of developing ATL is estimated to be approximately 2.5–5% [5,6]. ATL includes a spectrum of diseases that are referred to as smoldering-, chronic-, lymphoma-, and acute-type [7,8]. The chronic and smoldering types of ATL are considered indolent and are usually managed with watchful waiting until the disease progresses to aggressive (lymphoma- or acute-type) ATL [9]. Because the prognosis of ATL is poor with current treatment strategies, factors to forecast progression to ATL from asymptomatic carriers (ACs) have been researched [10–13] in the hope that they will be useful for preventive therapy under development in the early malignant stage.

Various cellular dysfunctions induced by viral genes (*e.g.*, tax and HBZ), genetic and epigenetic alterations, and the host immune system are considered to cooperatively contribute to leukemogenesis in ATL [14–16]. However, the complex mechanism may hinder determination of a clear mechanism of the pathology and make discovery of risk factors difficult. In a prospective nationwide study in Japan, high proviral load (VL,

Table 1. Clinical profile of patients infected with HTLV-I and normal controls.

Clinical sutype	Number of cases	Male	Female	Age (range)	WBC(/μl) (range)	Lymphocytes(%) (range)	Abnormal lymphocytes(%) (range)
HTLV-1 AC	40	12	28	49.9	5525	35.9	0.9
				(28–70)	(2680–10360)	(22.4–59.5)	(0.0–4.4)
Smoldering	7	4	3	55.3	5944	32.5	5.8
				(43–77)	(3680–8710)	(13.4–47.5)	(0.7–16.5)
Chronic	7	4	3	52.7	9180	45.8	9.2
				(37–60)	(4070–12790)	(35.0–61.5)	(3.4–12.7)
Acute	13	4	9	58.8	15328	16.3	40.3
				(42–74)	(4450–41480)	(1.7–50.5)	(3.0–89.6)
Normal controls	10	6	4	47.4	ND	ND	ND
				(27–66)			

WBC: white blood cells (normal range, 3500–9100/μl).
AC: asymptomatic carrier.
ND: analysis were not performed.
Average of age, WBC, lymphocytes (%) and abnormal lymphocytes (%) are shown.
The proportion of abonormal lymphocytes in peripheral blood WBCs was evaluated by morphological exmanination.
doi:10.1371/journal.pone.0053728.t001

over 4.17 copies/100 peripheral blood mononuclear cells) was found to be a major risk factor for HTLV-I AC developing into ATL [13]. Although VL indicates the proportion of HTLV-I-infected cells, it does not indicate size or degree of malignant progression in each clone; *i.e.*, it does not directly indicate progression of disease stage in HTLV-I infection. Moreover, the majority of ACs with high VL remained intact during the study period, indicating that a more accurate indicator of progression is needed.

In our recent study to purify monoclonal ATL cells from acute-type patients by flow cytometry, three subpopulations were observed in a CD3 versus CD7 plot of $CD4^+$ cells (H: $CD3^{high}CD7^{high}$, D: $CD3^{dim}CD7^{dim}$, L: $CD3^{dim}CD7^{low}$), and the majority of ATL cells were enriched in the L subpopulation [17]. Clonality analyses revealed that the D and L subpopulations contained the same clone, suggesting clonal evolution of HTLV-I-infected cells to ATL cells. From these findings, we speculated that the CD3 versus CD7 profile may reflect disease progression in HTLV-I infection. In this study, the CD3 versus CD7 profile by flow cytometry, combined with molecular (clonality and proviral load) characterizations, were analyzed in patients with various clinical subtypes (HTLV-I AC, and indolent and aggressive ATL). We found that the CD3 versus CD7 profile reflected disease progression of HTLV-I-infected cells to ATL cells. We also discuss the significance of this analysis as a novel risk indicator for HTLV-I ACs in forecasting progression to ATL.

Materials and Methods

Cell lines and patient samples

TL-Om1, an HTLV-I-infected cell line, established Dr. Hinuma's laboratory [18], was provided by Dr. Toshiki Watanabe (The University of Tokyo, Tokyo, Japan) and was cultured in RPMI-1640 medium containing 10% fetal bovine serum. Peripheral blood samples were collected from inpatients and outpatients at our hospital from August 2009 to November 2011. All patients with ATL were categorized according to Shimoyama's criteria [7,8]. Patients with various complications, such as autoimmune disorder and systemic infections, were excluded. Lymphoma-type patients were excluded because ATL cells are not considered to exist in peripheral blood of this clinical subtype. In patients with ATL receiving chemotherapy, blood samples were collected before treatment or during the recovery phase between chemotherapy sessions. Samples collected from 10 healthy volunteers (mean age: 47.4 years; range: 27–66 years) were used as normal controls.

The present study was approved by the research ethics committee of the institute of medical science, the university of Tokyo. Subjects provided written informed consent.

Flow cytometry and cell sorting

Peripheral blood mononuclear cells (PBMCs) were isolated from heparin-treated whole blood by density gradient centrifugation, as described previously [17]. Cells were stained using a combination of phycoerythrin (PE)-CD7, APC-Cy7-CD3, Pacific Blue-CD4, and Pacific Orange-CD14. Pacific Orange-CD14 was purchased from Caltag-Invitrogen (Carlsbad, CA). All other antibodies were obtained from BD BioSciences (San Jose, CA). Propidium iodide (PI; Sigma, St. Louis, MO) was added to the samples to stain dead cells immediately prior to flow cytometry. A BD FACS Aria instrument (BD Immunocytometry Systems, San Jose, CA) was used for all multicolor flow cytometry and cell sorting. Data were analyzed using the FlowJo software (Treestar, San Carlos, CA).

Quantification of HTLV-I proviral load by real-time quantitative polymerase chain reaction (PCR)

The HTLV-I proviral load in FACS-sorted PBMCs was quantified by real-time quantitative polymerase chain reaction (PCR; TaqMan method) using the ABI Prism 7000 sequence detection system (Applied Biosystems, Foster City, CA) as described previously [13,17]. Briefly, 50 ng of genomic DNA was extracted from human PBMCs using a QIAamp DNA blood Micro kit (Qiagen, Hilden, Germany). Triplicate samples of the DNA were amplified. Each PCR mixture, containing an HTLV-I pX region-specific primer pair at 0.1 μM (forward primer 5′-CGGATACCCAGTCTACGTGTT-3′ and reverse primer 5′-

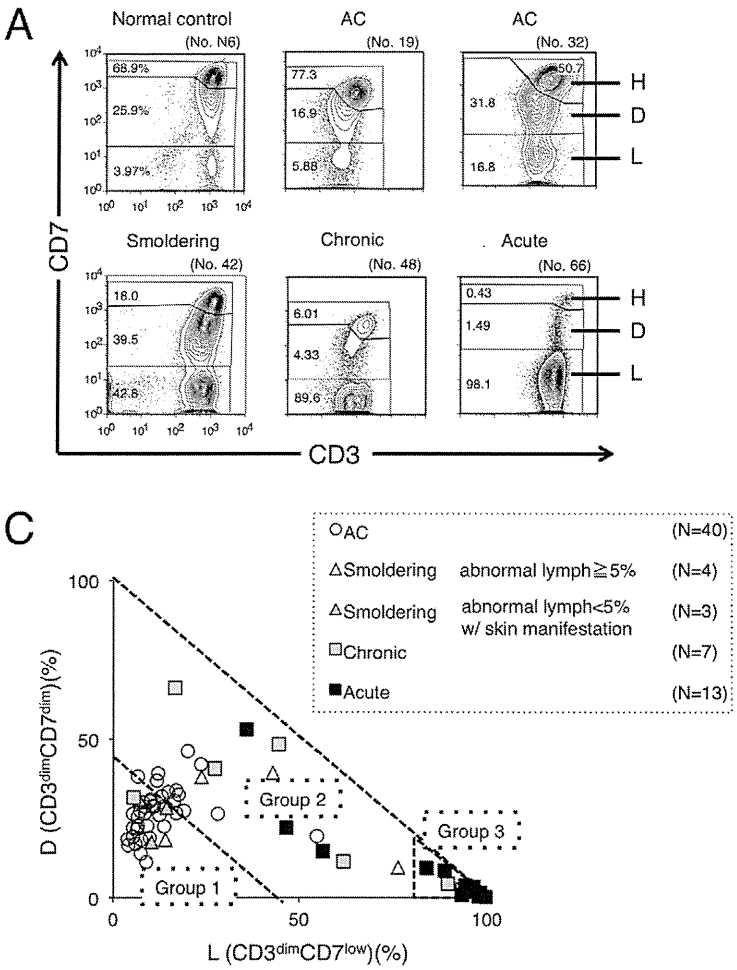

Figure 1. CD3 versus CD7 plots in flow cytometric analysis of patients who are asymptomatic HTLV-I carriers (ACs) and have various clinical subtypes of adult T-cell leukemia-lymphoma (ATL) suggest disease progression in HTLV-I infection. (A) Flow cytometric profile of an AC, various clinical subtypes of ATL (smoldering, chronic, and acute), and a normal control. Representative cases of CD3 versus CD7 plots in $CD4^+$ cells are shown. (B) A two-dimensional plot of AC cases showing the percentage of the D and L subpopulations by flow cytometry. AC cases were divided into two groups according to HTLV-I VL (greater or less than 4%). The border line (45% of D+L subpopulations) between Group 1 and 2 was set based on proviral load (VL). All AC cases with less than 4% VL were included in Group 1. All AC cases included in Group 2 had greater than 4% VL. VL<4%: n = 21; VL>4%: n = 19. All VL data in this figure were provided from the database of the Joint Study on Predisposing Factors of ATL Development (JSPFAD). (C) A two-dimensional plot of all patients showing the percentage of the D and L subpopulations. The smoldering type was divided into two categories: smoldering type with greater than 5% abnormal lymphocytes and smoldering type with less than 5% abnormal lymphocytes with skin manifestation. The two diagonal dotted lines indicate 45% and 100% of D+L subpopulations (*i.e.*, 55% and 0% of the H subpopulation). Data were categorized into three groups.
doi:10.1371/journal.pone.0053728.g001

CAGTAGGGCGTGACGATGTA-3′), FAM-labeled probe at 0.1 μM (5′- CTGTGTACAAGGCGACTGGTGCC-3′), and 1× TaqMan Universal PCR master mix (Applied Biosystems), was subjected to 50 cycles of denaturation (95°C, 15 seconds) and annealing to extension (60°C, 1 minute), following an initial Taq polymerase activation step (95°C, 10 minutes). The RNase P control reagent (Applied Biosystems) was used as an internal control for calculating the input cell number (using VIC reporter dye). DNAs extracted from TL-Om1 and normal human PBMCs were used as positive and negative controls, respectively. The HTLV-I proviral load (%) was calculated as the copy number of the pX region per input cell number. To correct the deviation of data acquired in each experiment, data from TL-Om1 (positive control) were adjusted to 100%, and the sample data were corrected accordingly by a proportional calculation.

Inverse long PCR

For clonality analysis, inverse long PCR was performed [17]. First, 1 μg of genomic DNA extracted from the FACS-sorted cells was digested with *Eco*RI and *Pst*I at 37°C overnight. Purification of DNA fragments was performed using a QIAEX2 gel extraction kit (Qiagen). The purified DNA was self-ligated with T4 DNA ligase (Takara Bio, Otsu, Japan) at 16°C overnight. The circular DNA obtained from the *Eco*RI digestion fragment was then digested

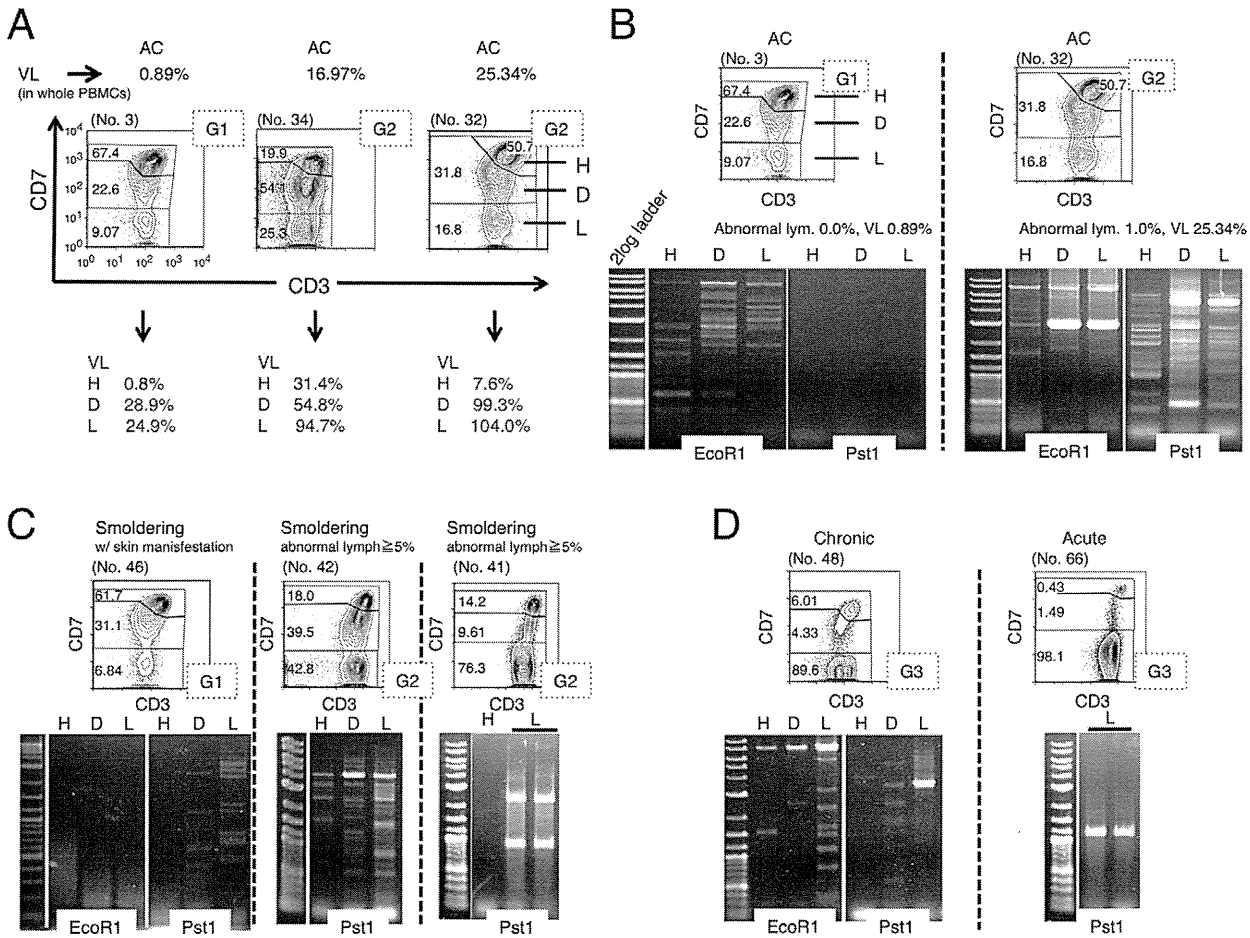

Figure 2. HTLV-I proviral load (VL) and clonality in each subpopulation, based on the CD3 versus CD7 plot. (A) The three subpopulations (H, D, L) based on the CD3 versus CD7 plot were subjected to fluorescence-activated cell sorting (FACS) and VL analysis. Three representative cases are shown. G1 or G2 in the dotted box indicates Group 1 or Group 2, categorized by the percentage of the D and L subpopulations, respectively. (B)–(D) Analysis of clonality in the three subpopulations based on the CD3 versus CD7 plot. Genomic DNA was extracted from FACS-sorted cells of each subpopulation and subjected to inverse long polymerase chain reaction (PCR). Representative data of two cases of AC (B), three cases of smoldering type, including one with skin manifestations (C), and cases of a chronic type and an acute type (D) are shown. PCR was performed in duplicate (black bars) in cases when a sufficient amount of DNA was obtained.
doi:10.1371/journal.pone.0053728.g002

with *Mlu*I, which cuts the pX region of the HTLV-I genome and prevents amplification of the viral genome. Inverse long PCR was performed using Takara LA *Taq* polymerase (Takara Bio). For the *Eco*RI-treated template, the forward primer was 5′-TGCCTGACCCTGCTTGCTCAACTCTACGTCTTTG-3′ and the reverse primer was 5′-AGTCTGGGCCCT-GACCTTTTCAGACTTCTGTTTC-3′. For the *Pst*I-treated group, the forward primer was 5′-CAGCCCATTCTATAG-CACTCTCCAGGAGAG-3′ and the reverse primer was 5′-CAGTCTCCAAACACGTAGACTGGGTATCCG-3. Each 50-μL reaction mixture contained 0.4 mM of each dNTP, 25 mM $MgCl_2$, 10× LA PCR buffer II containing 20 mM Tris-HCl and 100 mM KCl, 0.5 mM of each primer, 2.5 U LA *Taq* polymerase, and 50 ng of the processed genomic DNA. The reaction mixture was subjected to 35 cycles of denaturation (94°C, 30 seconds) and annealing to extension (68°C, 8 minutes). Following PCR, the products were subjected to electrophoresis on 0.8% agarose gels. In samples from which a sufficient amount of DNA was extracted, PCRs were performed in duplicate.

Results

CD3 versus CD7 profile in flow cytometry in various clinical subtypes of patients infected with HTLV-I

The clinical profiles of the 77 cases analyzed in this study are shown in Table 1. According to the gating procedure, as shown in Figure S1 [17], we constructed a CD3 versus CD7 plot of $CD4^+$ cells in PBMCs of various clinical subtypes from patients infected with HTLV-I and normal controls. The three subpopulations ($CD3^{high}CD7^{high}$, $CD3^{dim}CD7^{dim}$, and $CD3^{dim}CD7^{low}$) observed are referred to as the H, D, and L subpopulations, respectively. Representative results for each clinical subtype of HTLV-I infection are shown in Figure 1A. Regarding the data for an acute-type patient (no. 66), the dominant population was the L subpopulation, in which we previously demonstrated that monoclonal ATL cells are enriched [17]. Regarding the AC (no. 19), the CD3 versus CD7 profile was close to that of the normal control, although in some AC cases, such as no. 32, the profile differed from that of the normal control, because in contrast to case no. 19,

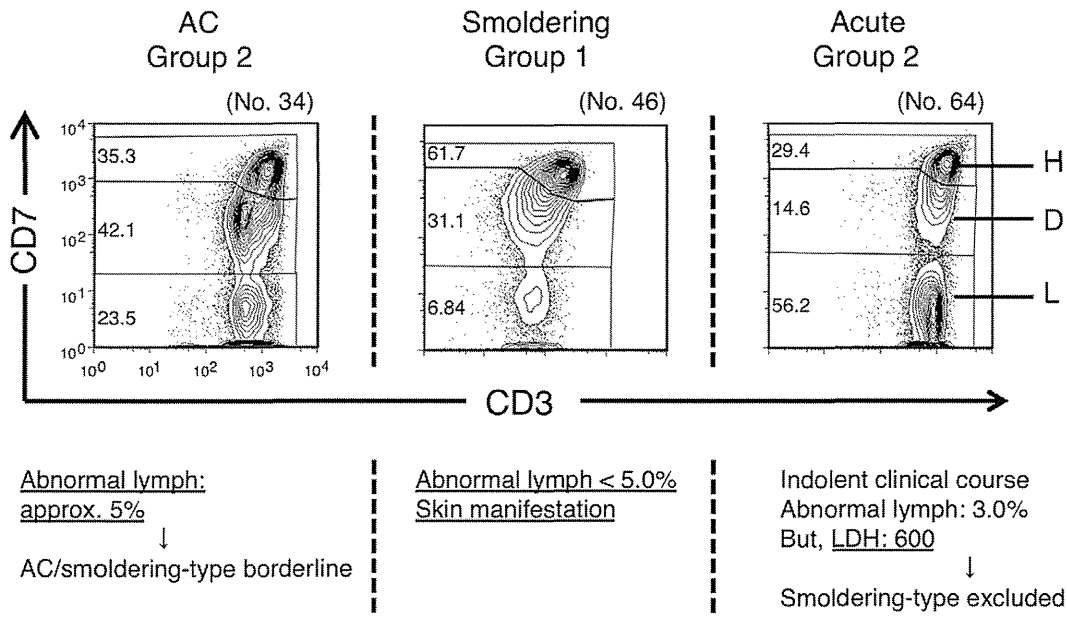

Figure 3. Study of exceptional cases categorized by proportion of the $CD3^{dim}CD7^{dim}$ (D) and $CD3^{dim}CD7^{low}$ (L) subpopulations. Left: An HTLV-I AC patient who was categorized in Group 2 in the D(%) versus L(%) plot. Middle: A patient with smoldering-type ATL who was categorized in Group 1. Right: A patient with acute-type ATL who was categorized in Group 2.
doi:10.1371/journal.pone.0053728.g003

these cases had increased D and L subpopulations. Regarding the data for indolent-type disease (smoldering and chronic), increases in the D and L subpopulations were intermediate between ACs and patients with acute-type disease. These representative flow cytometric data suggest that continuity in the CD3 versus CD7 profile seemed to exist among the various clinical subtypes of patients infected with HTLV-I.

The proportions of D and L subpopulations in all AC cases analyzed are shown in Figure 1B. Because the high HTLV-I proviral load (VL) in whole PBMCs, a VL of >4%, was reported to be a major risk indicator for progression to ATL [13], a border line was set based on VL. Group 1, the area under the diagonal line (D+L = 45%), included all AC cases with VLs of <4%. ACs with VLs of >4% were distributed between Groups 1 and 2. The proportions of D and L subpopulations in normal controls are shown in Figure S2. In this plot, all data for normal controls were distributed in Group 1. Data for all clinical subtypes are shown in Figure 1C. Most data for acute-type patients were located in the area beyond 80% of the L subpopulation and we designated this area as Group 3. Group 2, which is located between Group 1 and Group 3, included the majority of indolent-type (smoldering and chronic) cases. From these results, the three groups in the D(%) versus L(%) plot seemed to represent disease stage in each case.

Proviral load and clonality in each subpopulation in the CD3 versus CD7 plot

To further characterize each subpopulation (H, D, and L) in the CD3 versus CD7 plot, cells in each subpopulation were FACS-sorted and subjected to analysis of VL to determine the percentage of HTLV-I-infected cells in each subpopulation. Results for representative cases are shown in Figure 2A. The VL in whole PBMCs of an AC (no. 3) was low (0.89%). As expected, the VL in H, the major subpopulation, was low (0.8%). However, VLs in the D and L subpopulations were considerably higher (28.9% and 24.9%, respectively), indicating that HTLV-I-infected cells are relatively concentrated in these subpopulations. In the cases with high VLs in whole PBMCs (no. 32 with 25.34%; no. 34 with 16.97%), the VLs were also higher in the D and L subpopulations, and almost all cells in the L subpopulation were HTLV-I-infected.

In HTLV-I infection, progression to ATL requires several pathological steps, including clonal expansion [15]. To further characterize the three subpopulations based on the CD3 versus CD7 plot, we analyzed clonality in each subpopulation in patients with various clinical subtypes using the inverse long PCR method. Figure 2B shows two cases of AC. In the left case (no. 3), included in Group 1 in the D(%) and L(%) plot, multiple bands suggestive of multiple small clones were detected in the three subpopulations. However, no major band suggestive of a dominant clone was observed. In the right case (no. 32), included in Group 2, inverse long PCR of the FACS-sorted subpopulations suggested that the D and L subpopulations contained a major clone (Figure 2B). The D subpopulation had bands of the same size as those of the L subpopulation, indicating that the two distinct subpopulations contained a common major clone. Eleven cases of AC were included in Group 2. All three cases analyzed by Southern blotting (whole blood samples) were positive for clonal bands (Figure S3). In Figure 2C, data for three smoldering cases are shown. In case no. 46 (left), whose only manifestation was a skin eruption with few abnormal lymphocytes (less than 5% of white blood cells) in the peripheral blood, only faint minor bands suggestive of small clones were observed. In contrast, in the other two cases (nos. 42 and 41), intense bands suggestive of major clones were observed in both the D and L subpopulations. In no. 41 (right), weak bands were not visible, which suggested the selection of dominant clones. In Figure 2D, data for a chronic-type case and an acute-type case are shown. In both cases, intense bands in the L subpopulation suggest the existence of a major clone. The series of clonality analyses indicated that a major clone became more evident and the clinical

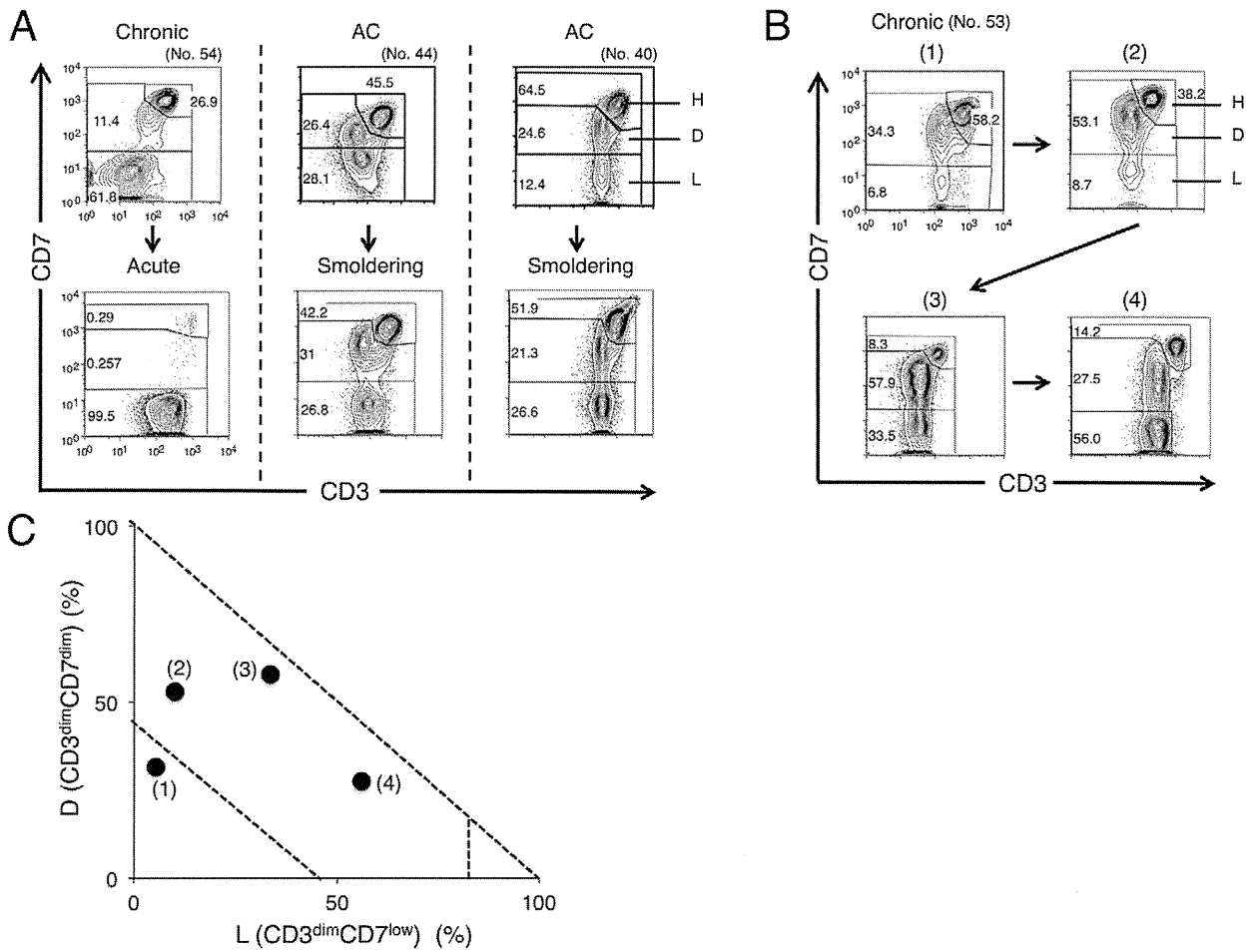

Figure 4. Alteration in the CD3 versus CD7 profile by flow cytometry in accordance with disease progression. (A) Change in the CD3 versus CD7 profile in representative cases. In all three cases shown, change in clinical data (*e.g.*, abnormal lymphocyte, LDH) resulted in progression of the clinical subtype. (B) Change in the CD3 versus CD7 profile in a time course in the case of chronic-type ATL. Clinical data are shown in Table S1. (C) Flow cytometric data in (B) are summarized in the D(%) versus L(%) plot.
doi:10.1371/journal.pone.0053728.g004

stage became more advanced as the D and L subpopulations increased.

Clinical evaluation of exceptional cases categorized by proportions of the $CD3^{dim}CD7^{dim}$ (D) and $CD3^{dim}CD7^{low}$ (L) subpopulations

As noted above, the D(%) versus L(%) plot generally represented disease stage in HTLV-I infection. However, we observed one case of chronic-type disease and three cases of smoldering-type disease in Group 1 and three cases of acute-type disease in Group 2. Furthermore, some ACs with VLs of >4% were observed in Group 2. Representative data from these apparently exceptional cases are shown in Figure 3. On the left, a case of AC (no. 34) observed in Group 2 is shown. 4.7% of lymphocytes in this blood sample were abnormal and clonality analysis by Southern blotting showed oligoclonal bands suggestive of clones of substantial size (Figure S3). These clinical data suggest that the disease stage would be around the AC/smoldering borderline. In the middle, a case of a smoldering type (no. 46) observed in Group 1 is shown. In this case, the percentage of abnormal lymphocytes in the peripheral blood was only 1%, but she had a histologically proven ATL lesion in the skin and was diagnosed with smoldering-type ATL. The other two smoldering cases categorized in Group 1 were the same as this case. These results indicate that ATL cells in these three smoldering cases infiltrated the skin, but not the peripheral blood. On the right, a case of acute-type disease categorized as Group 2 (no. 64) is shown. The clinical course of this patient was relatively indolent compared with typical acute-type disease. He had skin infiltration of ATL cells, but no lymph node swelling. However, LDH exceeded 1.5 times the upper limit of the normal range, which excludes a diagnosis of smoldering-type disease. Other acute-type cases categorized in Group 2 were diagnosed as such according to Shimoyama's criteria, but also had the same indolent clinical course as case no. 64. These cases should have been regarded as indolent ATL.

Changes in the CD3 versus CD7 profile in flow cytometry with disease progression

In several cases, we could obtain time-sequential samples (Figure 4). The patient (no. 54) shown on the left in Figure 4A progressed from chronic-type to acute-type disease. In flow cytometric analysis, decreases in the H and D subpopulations

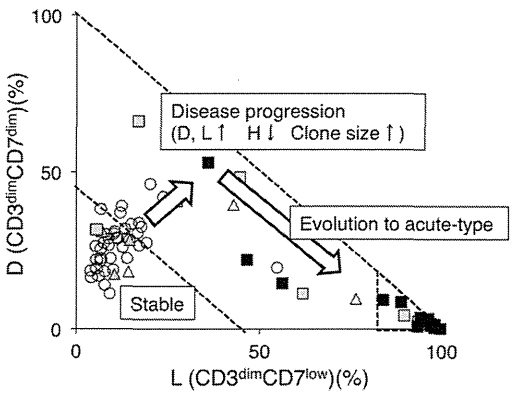

Figure 5. Summary of the study: the CD3 versus CD7 profile reflects progression of disease stage in patients infected with HTLV-I. In the percentage of D ($CD3^{dim}CD7^{dim}$) versus L ($CD3^{dim}CD7^{low}$) plot, Group 1 includes the majority of AC cases. As disease stage progresses, the CD3 versus CD7 profile then changes. With downregulation of CD3 and CD7, the D and L subpopulations increase gradually (Group 2). During this step, clones in the D and L subpopulations increase in size. Further accumulation of genetic alterations will result in rapid expansion of ATL clones—*i.e.*, evolution to acute-type ATL. In this step, the CD3 versus CD7 profile will progress from Group 2 to 3.
doi:10.1371/journal.pone.0053728.g005

and an increase in the L subpopulation were observed, indicating that disease progression correlated well with the change in the CD3 versus CD7 profile. The patients in the middle (no. 44) and on the right (no. 40) were included in Group 2 at the AC stage and later progressed to smoldering-type ATL. Although variation in the change of the flow cytometric profile was seen between these patients, the results suggest that ACs in Group 2 are at high risk of developing ATL.

The patient in Figure 4B (no. 53) was initially diagnosed with AC and later progressed to chronic-type ATL. Although the initial clinical course was stable, an increase in abnormal lymphocyte numbers was later observed, and low-dose VP-16 therapy (50 mg/day) was initiated because of hypoxemia due to lung infiltration of ATL cells. Table S1 and Figure 4C show summaries of the clinical data and the flow cytometric analyses, respectively. The flow cytometric data correlated well with disease progression.

Discussion

Findings in our previous analysis of acute-type ATL samples prompted our analysis of various clinical subtypes of patients infected with HTLV-I to examine whether the CD3 versus CD7 profile reflects the progression of oncogenesis in HTLV-I-infected cells [17]. Representative flow cytometric data shown in Figure 1A suggested that the CD3 versus CD7 profile changed during disease progression. As the disease stage progressed, the D and L subpopulations increased with concomitant decreases in the $CD3^{high}CD7^{high}$(H) subpopulation. Figure 1C, a summary of the flow cytometric data of all cases analyzed, reveals that the two-dimensional plot of the proportions of the D versus L subpopulations could divide all cases into three groups. Group 1, the area under the diagonal line, equivalent to 55% of the H subpopulation in which all normal controls were included (Figure S2), contained the majority of HTLV-I ACs. Group 3 was the area beyond 80% of the L subpopulation, and the majority of acute-type cases were included in this group. Group 2, located between Groups 1 and 3 (*i.e.*, less than 55% of the H subpopulation and 80% of the L subpopulation), included indolent-type (smoldering and chronic) cases and some AC cases. These results suggest that the CD3 versus CD7 expression profile reflects disease stage. Initially, both the D and L subpopulations gradually and simultaneously increased. However, at the clinically advanced stage, the increase in the L subpopulation was prominent. The change is considered to reflect the biological difference between the D and L subpopulations, which needs to be clarified.

In HTLV-I infection, the small clones of infected cells are considered to coexist from the AC stage [19,20]. A selected clone from the multiple small clones then grows and progresses to the malignant state, and the emergence of a dominant clone indicates disease progression in ATL [19,20]. As shown in Figure 2B–D, major bands suggesting dominant clones were evident in patients with progressed clinical subtypes or those in the advanced group in the CD3 versus CD7 profile, and major bands existed exclusively in the D and L subpopulations. These data also support the idea that increases in the D and L subpopulations correlate with the progression of disease stage. AC cases in Group 2 had high HTLV-I proviral loads (>4%; Figure 1B) and clear major bands were observed by inverse long PCR in these cases (Figure 2B, right). Sasaki *et al.* reported that two cases of HTVL-I AC with oligoclonal bands on Southern blots and high VLs (20%) had progressed to ATL by 4 and 3.5 years later [21]. The two cases may correspond to HTLV-I AC in Group 2 proposed in our study. In fact, two cases of ACs in our series that were included in Group 2 progressed to smoldering ATL (Figure 4A). AC cases in Group 2 could be regarded as advanced carriers. Our flow cytometric analysis could apparently discriminate high-risk AC cases from stable ones. Follow-up analysis of these cases is warranted to determine whether AC cases included in Group 2 progress to ATL. Flow cytometric data for these AC cases included in Group 2 (Figure 1A and 1C) were similar to those for indolent ATL cases in Group 2. These ACs in Group 2 can be considered essentially the same as smoldering ATL cases. Some of the ACs categorized according to Shimoyama's criteria should in fact be separated and regarded as a subtype together with at least some of the smoldering ATL cases.

Iwanaga *et al.* reported that high HTLV-I proviral load (>4%) in whole PBMCs was a risk factor for progression to ATL [13]. In Figure 1B, the ACs with VLs>4% were distributed between Groups 1 and 2. These findings suggest that not all ACs with high VLs are currently in an advanced stage, although they may have the potential to develop ATL in the future.

In general, the categorization by flow cytometric profile correlated well with the current classification of clinical subtypes, with some exceptional cases of acute-type and smoldering-type disease (Figure 3). The only manifestation of three smoldering cases categorized in Group 1 was skin lesions; they fell into Group 1 because they showed minimal abnormalities in peripheral blood [22]. Three acute-type ATL cases categorized in Group 2 had indolent clinical courses. A diagnosis of acute-type disease is made when the indolent-type and lymphoma-type are excluded, according to Shimoyama's criteria. The CD3 versus CD7 plot may discriminate the cases that will follow an indolent clinical course from the aggressive acute-type ATL.

The VL in each subpopulation indicated that HTLV-I-infected cells were relatively concentrated in the D and L subpopulations (representative data are shown in Figure 2A). These data are consistent with downregulation of CD3 and CD7 being relevant to HTLV-I infection, although cells without HTLV-I infection may also contribute to this change to some extent, as a substantial subpopulation of T cells has been reported to be CD7-deficient under physiological [23,24] and certain pathological conditions,

including autoimmune disorders and viral infection [25–29]. To more precisely analyze phenotypic changes in HTLV-I-infected cells, markers that indicate HTLV-I infection should be incorporated in future studies.

A summary of this study is shown in Figure 5. In the CD3 versus CD7 profile, most AC cases were included in Group 1, in which the D and L subpopulations were relatively small. Consistent with disease progression to smoldering- and chronic-type ATL, a decrease in the H subpopulation and increases in the D and L subpopulations occur (Group 2). In this step, increases in the sizes of clones in the D and L subpopulations are observed. Further expansion of the leukemic clone results in progression to acute-type ATL in which the L subpopulation has expanded (Group 3). According to a study by Yamaguchi *et al.*, the natural course of ATL is to progress from the HTLV-I carrier state through the intermediate state, smoldering ATL, and chronic ATL, and finally to the acute ATL, indicating a process of multistage leukemogenesis [19]. We consider this study to successfully link the progressive clinical status and phenotypic changes in HTLV-I-infected cells. However, the way in which this profile reflects multistep oncogenesis in HTVL-I infection at the molecular level remains unclear. Further molecular analyses of the three subpopulations will help in understanding the mechanism(s).

Supporting Information

Figure S1 Representative flow cytometric analysis of an HTLV-I asymptomatic carrier (patient no. 32). The CD3 versus CD7 plot of $CD4^+$ cells was constructed according to the gating procedure shown in this figure. In the plot, we designated three subpopulations: H ($CD3^{high}CD7^{high}$), D ($CD3^{dim}CD7^{dim}$), and L ($CD3^{dim}CD7^{low}$).
(PPTX)

Figure S2 A two-dimensional plot of 10 normal controls showing the percentage of the D and L subpopulations.
(PPTX)

Figure S3 Southern blot analysis of clonal integration of the HTLV-I provirus. Representative data (AC, No. 34) are shown. In *Eco*RI or *Pst*I digestion, a band indicated by a red arrow represents the monoclonal integration of the provirus. The band pattern indicates that two major clones coexist. This analysis was performed by a commercial laboratory (SRL, Tokyo, Japan).
(PPTX)

Table S1 Clinical data in a case of chronic-type ATL (No. 53). Proportion of abonormal lymphocytes in the preipheral blood WBC were evaluated by morphological exmanination. LDH: Lactate dehydrogenase (normal range, 120–240 U/L) sIL-2R: soluble interleukin-2 receptor (normal range, 122–496 U/ml).
(XLSX)

Acknowledgments

We thank Dr. Toshiki Watanabe, Dr. Kazumi Nakano, and Dr. Tadanori Yamochi (The University of Tokyo) for providing the TL-Om1 cell line and the plasmid containing the HTLV-I genome, which was used as a standard for the quantification of proviral load. We also thank Mr. Yuji Zaike (Clinical Laboratory, Research Hospital, Institute of Medical Science, The University of Tokyo) for his excellent technical advice. We are grateful to the hospital staff who have made a commitment to providing high-quality care to all of our patients.

Author Contributions

Conceived and designed the experiments: KT AT KU. Performed the experiments: SK YT. Analyzed the data: EW NW TI NO. Contributed reagents/materials/analysis tools: MI MT KU NO. Wrote the paper: SK KU.

References

1. Yoshida M, Miyoshi I, Hinuma Y (1982) Isolation and characterization of retrovirus from cell lines of human adult T-cell leukemia and its implication in the disease. Proc Natl Acad Sci U S A 79: 2031–2035.
2. Osame M, Usuku K, Izumo S, Ijichi N, Amitani H, et al. (1986) HTLV-I associated myelopathy, a new clinical entity. Lancet 1: 1031–1032.
3. Mochizuki M, Watanabe T, Yamaguchi K, Takatsuki K, Yoshimura K, et al. (1992) HTLV-I uveitis: a distinct clinical entity caused by HTLV-I. Japanese journal of cancer research : Gann 83: 236–239.
4. Proietti FA, Carneiro-Proietti AB, Catalan-Soares BC, Murphy EL (2005) Global epidemiology of HTLV-I infection and associated diseases. Oncogene 24: 6058–6068.
5. Yamaguchi K, Watanabe T (2002) Human T lymphotropic virus type-I and adult T-cell leukemia in Japan. International journal of hematology 76 Suppl 2: 240–245.
6. Murphy EL, Hanchard B, Figueroa JP, Gibbs WN, Lofters WS, et al. (1989) Modelling the risk of adult T-cell leukemia/lymphoma in persons infected with human T-lymphotropic virus type I. International journal of cancer Journal international du cancer 43: 250–253.
7. Shimoyama M (1991) Diagnostic criteria and classification of clinical subtypes of adult T-cell leukaemia-lymphoma. A report from the Lymphoma Study Group (1984–87). Br J Haematol 79: 428–437.
8. Tsukasaki K, Hermine O, Bazarbachi A, Ratner L, Ramos JC, et al. (2009) Definition, prognostic factors, treatment, and response criteria of adult T-cell leukemia-lymphoma: a proposal from an international consensus meeting. J Clin Oncol 27: 453–459.
9. Takasaki Y, Iwanaga M, Imaizumi Y, Tawara M, Joh T, et al. (2010) Long-term study of indolent adult T-cell leukemia-lymphoma. Blood 115: 4337–4343.
10. Hisada M, Okayama A, Shioiri S, Spiegelman DL, Stuver SO, et al. (1998) Risk factors for adult T-cell leukemia among carriers of human T-lymphotropic virus type I. Blood 92: 3557–3561.
11. Imaizumi Y, Iwanaga M, Tsukasaki K, Hata T, Tomonaga M, et al. (2005) Natural course of HTLV-1 carriers with monoclonal proliferation of T lymphocytes ("pre-ATL") in a 20-year follow-up study. Blood 105: 903–904.
12. Kamihira S, Atogami S, Sohda H, Momita S, Yamada Y, et al. (1994) Significance of soluble interleukin-2 receptor levels for evaluation of the progression of adult T-cell leukemia. Cancer 73: 2753–2758.
13. Iwanaga M, Watanabe T, Utsunomiya A, Okayama A, Uchimaru K, et al. (2010) Human T-cell leukemia virus type I (HTLV-1) proviral load and disease progression in asymptomatic HTLV-1 carriers: a nationwide prospective study in Japan. Blood 116: 1211–1219.
14. Okamoto T, Ohno Y, Tsugane S, Watanabe S, Shimoyama M, et al. (1989) Multi-step carcinogenesis model for adult T-cell leukemia. Japanese journal of cancer research : Gann 80: 191–195.
15. Matsuoka M, Jeang KT (2007) Human T-cell leukaemia virus type 1 (HTLV-1) infectivity and cellular transformation. Nat Rev Cancer 7: 270–280.
16. Yoshida M (2010) Molecular approach to human leukemia: isolation and characterization of the first human retrovirus HTLV-1 and its impact on tumorigenesis in adult T-cell leukemia. Proceedings of the Japan Academy Series B, Physical and biological sciences 86: 117–130.
17. Tian Y, Kobayashi S, Ohno N, Isobe M, Tsuda M, et al. (2011) Leukemic T cells are specifically enriched in a unique CD3(dim) CD7(low) subpopulation of CD4(+) T cells in acute-type adult T-cell leukemia. Cancer science 102: 569–577.
18. Sugamura K, Fujii M, Kannagi M, Sakitani M, Takeuchi M, et al. (1984) Cell surface phenotypes and expression of viral antigens of various human cell lines carrying human T-cell leukemia virus. International journal of cancer Journal international du cancer 34: 221–228.
19. Yamaguchi K, Kiyokawa T, Nakada K, Yul LS, Asou N, et al. (1988) Polyclonal integration of HTLV-I proviral DNA in lymphocytes from HTLV-I seropositive individuals: an intermediate state between the healthy carrier state and smouldering ATL. British journal of haematology 68: 169–174.
20. Mortreux F, Gabet AS, Wattel E (2003) Molecular and cellular aspects of HTLV-1 associated leukemogenesis in vivo. Leukemia : official journal of the Leukemia Society of America, Leukemia Research Fund, UK 17: 26–38.
21. Sasaki D, Doi Y, Hasegawa H, Yanagihara K, Tsukasaki K, et al. (2010) High human T cell leukemia virus type-1(HTLV-1) provirus load in patients with HTLV-1 carriers complicated with HTLV-1-unrelated disorders. Virology journal 7: 81.
22. Setoyama M, Katahira Y, Kanzaki T (1999) Clinicopathologic analysis of 124 cases of adult T-cell leukemia/lymphoma with cutaneous manifestations: the smouldering type with skin manifestations has a poorer prognosis than previously thought. The Journal of dermatology 26: 785–790.
23. Reinhold U, Abken H (1997) CD4+ CD7- T cells: a separate subpopulation of memory T cells? J Clin Immunol 17: 265–271.

24. Reinhold U, Abken H, Kukel S, Moll M, Muller R, et al. (1993) CD7- T cells represent a subset of normal human blood lymphocytes. J Immunol 150: 2081–2089.
25. Aandahl EM, Quigley MF, Moretto WJ, Moll M, Gonzalez VD, et al. (2004) Expansion of CD7(low) and CD7(negative) CD8 T-cell effector subsets in HIV-1 infection: correlation with antigenic load and reversion by antiretroviral treatment. Blood 104: 3672–3678.
26. Autran B, Legac E, Blanc C, Debre P (1995) A Th0/Th2-like function of CD4+CD7- T helper cells from normal donors and HIV-infected patients. J Immunol 154: 1408–1417.
27. Legac E, Autran B, Merle-Beral H, Katlama C, Debre P (1992) CD4+CD7-CD57+ T cells: a new T-lymphocyte subset expanded during human immunodeficiency virus infection. Blood 79: 1746–1753.
28. Schmidt D, Goronzy JJ, Weyand CM (1996) CD4+ CD7- CD28- T cells are expanded in rheumatoid arthritis and are characterized by autoreactivity. J Clin Invest 97: 2027–2037.
29. Willard-Gallo KE, Van de Keere F, Kettmann R (1990) A specific defect in CD3 gamma-chain gene transcription results in loss of T-cell receptor/CD3 expression late after human immunodeficiency virus infection of a CD4+ T-cell line. Proc Natl Acad Sci U S A 87: 6713–6717.

High-grade Lung Adenocarcinoma With Fetal Lung–like Morphology

Clinicopathologic, Immunohistochemical, and Molecular Analyses of 17 Cases

Shigeki Morita, MD,† Akihiko Yoshida, MD, PhD,*† Akiteru Goto, MD, PhD,†*
Satoshi Ota, MD, PhD,† Koji Tsuta, MD, PhD, Karin Yokozawa, BSc,* Hisao Asamura, MD, PhD,‡*
Jun Nakajima, MD, PhD,§ Daiya Takai, MD, PhD,‖ Masaya Mori, MD, PhD,¶
Teruaki Oka, MD,# Junichi Tamaru, MD, PhD,# Shinji Itoyama, MD, PhD,#
Koh Furuta, MD, PhD, Masashi Fukayama, MD, PhD,† and Hitoshi Tsuda, MD, PhD**

Abstract: Low-grade lung adenocarcinoma of fetal lung type, which is well characterized by its unique clinicopathologic and molecular features, is recognized as a distinct variant of lung cancer. In contrast, high-grade lung adenocarcinoma with fetal lung–like morphology (HG-LAFM) has not been studied widely. To characterize this subset better, we analyzed 17 high-grade adenocarcinomas with at least focal component resembling a developing epithelium in the pseudoglandular phase of the fetal lung. These rare (ca. 0.4%) carcinomas occurred predominantly in elderly men with a heavy smoking history, who showed elevated serum α-fetoprotein in 4 of 5 cases tested. Histologic examination revealed a fetal lung–like component as a focal finding accounting for 5% to 60% of the total tumor volume. It was invariably admixed with tissues having a morphology not resembling that of a fetal lung. A coexisting non–fetal lung–like element was quite heterogenous in appearance, showing various growth patterns. However, clear-cell (88%), hepatoid (29%), and large cell neuroendocrine carcinoma (24%) histology seemed overrepresented. HG-LAFM was characterized immunohistochemically by frequent expression of α-fetoprotein (41%), glypican-3 (88%), SALL-4 (59%), neuroendocrine markers (82%), CDX-2 (35%), and p53 (65%). HG-LAFM was molecularly heterogenous in that *EGFR* or *KRAS* mutation was observed in 22% of cases tested for both. Our data indicate that HG-LAFMs might form a coherent subgroup of lung adenocarcinomas. However, the uniformly focal nature of the fetal lung–like element, widely diverse coexisting non–fetal lung–like histology, and inhomogenous molecular profiles lead us to believe that HG-LAFM is best regarded as a morphologic pattern showing characteristic association with several clinicopathologic parameters rather than a specific tumor entity.

Key Words: lung, adenocarcinoma, fetal, neuroendocrine

(*Am J Surg Pathol* 2013;37:924–932)

Lung cancer is the leading cause of tumor mortality worldwide.[1] Adenocarcinoma, the most common subtype, is well known for its diverse morphologic appearance.[2] Primary lung adenocarcinomas can, but rarely, exhibit morphologic features resembling those of a developing fetal lung.[3–8] In 1998, Nakatani et al[8] reviewed 16 lung carcinomas with such features and subdivided them into low-grade and high-grade forms. Low-grade adenocarcinoma of fetal lung type (also known as pulmonary endodermal tumor resembling fetal lung[4]) was characterized by complex glandular structures resembling a developing epithelium in the pseudoglandular phase of the fetal lung, low nuclear atypia, and morule formation. In contrast, aside from the fetal lung–like epithelial character, the high-grade form was found to show prominent nuclear atypia, a lack of morules, a transition to conventional adenocarcinoma, and necrosis. This dichotomous classification was later applied to biphasic tumors conventionally known as "pulmonary blastoma." They were subdivided into "classic" type associated with low-grade fetal lung–like epithelium and "blastomatoid variant of carcinosarcoma" associated with high-grade fetal lung–like epithelium.[9]

Subsequent molecular studies have revealed that the low-grade adenocarcinoma of fetal lung type (and its biphasic variant) was characterized by β-catenin gene mutation leading to aberrant nuclear/cytoplasmic β-catenin

From the Departments of *Pathology and Clinical Laboratories; ‡Thoracic Oncology, Thoracic Surgery Division, National Cancer Center Hospital; †Department of Pathology, Graduate School of Medicine, The University of Tokyo; Departments of §Thoracic Surgery; ‖Clinical Laboratory, The University of Tokyo Hospital; ¶Mitsui Memorial Hospital, Tokyo; and #Department of Pathology, Saitama Medical Center, Saitama Medical University, Saitama, Japan.

Conflicts of Interest and Source of Funding: The authors have disclosed that they have no significant relationships with, or financial interest in, any commercial companies pertaining to this article.

Correspondence: Masashi Fukayama, MD, PhD, Department of Pathology, Graduate School of Medicine, The University of Tokyo, 7-3-1 Hongo, Bunkyo-ku, Tokyo 113-0033, Japan (e-mail: mfukayama-tky@umin.net).

expression.[9–11] Currently, low-grade adenocarcinoma of fetal lung type is recognized as a distinct subgroup of lung cancer in the current World Health Organization (WHO) classification by the name of well-differentiated fetal adenocarcinoma.[2] In contrast, the high-grade form, hereinafter termed high-grade lung adenocarcinoma with fetal lung–like morphology (HG-LAFM) in this article, has not been investigated widely. No systematic study of this subset has been undertaken since the original proposal by Nakatani et al,[8] and it remains unclear whether HG-LAFM is a distinct variant of lung cancer.

In this study, we examined clinicopathologic, immunohistochemical, and molecular features of 17 cases of HG-LAFM retrospectively to elucidate this morphologic subset and to determine whether HG-LAFM deserves designation as a specific variant of lung adenocarcinoma.

MATERIALS AND METHODS

Case Selection

This study was approved by the review board of each participating institution. HG-LAFMs were sought electronically from the respective surgical pathology archives of the National Cancer Center Hospital (Tokyo), The University of Tokyo Hospital (Tokyo), Mitsui Memorial Hospital (Tokyo), and Saitama Medical University (Saitama). The search was facilitated by key words such as "fetal," "primitive," and "immature." Fetal lung–like morphology was defined by complex glandular architecture composed of tall columnar cells that displayed supranuclear and/or subnuclear clear cytoplasm resembling a developing epithelium in the pseudoglandular phase of the fetal lung. Occasional papillary infoldings were allowed. The oval-shaped nucleus in each constituent tumor cell was typically aligned as perpendicular to the basement membrane. The apical border of tumoral glands was flat rather than interrupted by apical snouts. The nuclear grade was high. We required at least focal area of unequivocal fetal lung–like morphology for inclusion in this study. Two low-grade adenocarcinomas of fetal lung type (1 monophasic and 1 biphasic) in the archives were excluded. The search ultimately identified 17 cases of HG-LAFM, which accounted for ca. 0.4% of the >4000 primary lung cancer cases that had been surgically resected at the participating institutions.

Clinicopathologic Examination

Medical records were reviewed for demographic data, smoking history, serum α-fetoprotein (AFP) level when available, and follow-up information. Tumors were staged according to the TNM system.[12] All the tumors had been sampled adequately, fixed in 10% formalin, embedded in paraffin, cut into 4-μm-thick sections, and stained with hematoxylin and eosin for routine pathologic examination. All available glass slides were reviewed by 2 or 3 pathologists (S.M., A.G., and A.Y.). The amount of fetal lung–like element was evaluated as a percentage of the total tumor volume. Coexisting components that did not resemble developing fetal lung were also assessed and were classified on the basis of WHO guidelines.[2] The conventional adenocarcinoma component was characterized further by the growth pattern (lepidic, papillary, acinar, and solid) according to a recent recommendation.[13] In addition, we devoted attention to the presence or absence of hepatoid and clear-cell patterns and recorded these patterns separately. Although unrecognized in the present WHO scheme, a hepatoid pattern in lung adenocarcinoma was previously documented[14–17] and was defined by solid to trabecular growth of tumor cells having eosinophilic cytoplasm, thereby simulating hepatocellular carcinoma. A clear-cell pattern indicated tumor cells showing significantly clear cytoplasm irrespective of the growth pattern.[18] Because fetal lung–like tumor cells harbored clear cytoplasm by definition, we considered only non–fetal lung–like element with clear cytoplasm as a clear-cell pattern for evaluation. The relative amount of each non–fetal lung–like histologic pattern was expressed as a percentage of the total tumor volume. Lymphovascular invasion, pleural invasion, and necrosis were assessed. Metastatic tumor tissues in lymph nodes were also evaluated when available.

Immunohistochemistry

For immunohistochemical staining, primary antibodies for AFP, glypican-3 (GPC-3), SALL-4, synaptophysin, chromogranin A, neural cell adhesion molecule, thyroid transcription factor-1 (TTF-1), CDX-2, p53, and β-catenin were used (Table 1). Sections of 4 μm thickness from each block of the tumor tissue were stained using an automated stainer (Ventana Benchmark; Ventana Medical Systems Inc., Tucson, AZ) along with appropriate positive and negative controls.

All samples were evaluated and scored by 2 pathologists (S.M. and A.G.) without knowledge of clinicopathologic data. Staining of >1% of tumor cells was required for the positive designation except for p53, in which nuclear staining of >10% of tumor cells was considered positive.

Molecular Analysis

We performed a mutation analysis of epidermal growth factor receptor (*EGFR*) to detect deletion in exon 19 and point mutation in exon 21 (L858R) and of *KRAS* exon 2 (codons 12 and 13) and exon 3 (codon 61) by high-resolution melting analysis. DNA was extracted from archived formalin-fixed or methanol-fixed, paraffin-embedded tissues using the QIAamp DNA Micro Kit (Qiagen Inc., Valencia, CA), following the manufacturer's instructions. Polymerase chain reaction was performed to amplify exons 19 and 21 of *EGFR* and exons 2 and 3 of *KRAS* using LCGreen I (Idaho Technology, Salt Lake City, UT) on a thermal cycler. Primers for *EGFR* analysis were designed as described previously.[19] Primers for *KRAS* exon 3 analysis were commercially available (Idaho Technology), and primers for *KRAS* exon 2 (92 bp) were published previously by others.[20] An additional set of primers for *KRAS* exon 2 (62 bp) was

TABLE 1. Antibodies Used for Immunohistochemical Studies

Antibody	Clone	Type	Source	Dilution	Staining Pattern
AFP	—	Rabbit, poly	Dako, Glostrup, Denmark	1:1000	C
GPC-3	1G12	Mouse, mono	BioMosaics Inc., Burlington, VT	1:200	C, M
SALL-4	6E3	Mouse, mono	Abnova Corp., Taipei, Taiwan	1:100	N
Synaptophysin	—	Rabbit, poly	Dako	1:100	C
Chromogranin A	—	Rabbit, poly	Dako	1:200	C
NCAM (CD56)	1B6	Mouse, mono	Novocastra Laboratories Ltd., Newcastle, UK	1:50	M
TTF-1	8G7G3/1	Mouse, mono	Neomarkers, Fremont, CA	1:200	N
CDX-2	CDX-2-88	Mouse, mono	BioGenex, San Ramon, CA	1:50	N
p53	DO-7	Mouse, mono	Novocastra Laboratories Ltd.	1:100	N
β-catenin	14/ β-catenin	Mouse, mono	BD Transduction Laboratories, San Diego, CA	1:1000	N

C indicates cytoplasmic; M, membranous; N, nuclear; NCAM, neural cell adhesion molecule; poly, polyclonal; mono, monoclonal; TTF-1, thyroid transcription factor-1.

designed by one of the authors (K.Y.). The primer sequences are presented in Table 2. These polymerase chain reaction products were analyzed using the LightScanner platform (Idaho Technology). Data were acquired and analyzed using the accompanying software (Idaho Technology). After the normalization step, melting curve shapes of the tumor samples and control samples were compared. Human Genomic DNA (Roche Diagnostics Corp., Indianapolis, IN) was used as the negative control sample with wild-type *EGFR* and *KRAS*. All analyses were performed in a blinded manner to the clinicopathologic data.

Statistics

Three-year and 5-year overall survival and disease-free survival rates were calculated with the Kaplan-Meier method using software STAT View for Windows, ver. 5 (SAS Institute Inc., Cary, NC).

RESULTS

Clinical Characteristics

The clinical characteristics of HG-LAFMs are presented in Table 3. HG-LAFM almost exclusively occurred in men (16 men, 1 woman). The patient ages ranged from 40 to 75 years (median, 64.2 y). Except for 2 patients whose smoking history was unknown, all the patients had been heavy smokers with exposure of >20 pack-years (median, 54.9 p-y). Three patients were symptomatic at presentation with cough (cases 3 and 4) or chest pain (case 1). Serum AFP level was available in 5 cases, and it was elevated in 4 of them (case 8, 8720 ng/mL; case 12, 19 ng/mL; case 13, 16 ng/mL; case 17, 24 ng/mL, normal range: <10 ng/mL). All patients were treated with lobectomy and standard lymph node dissection with a curative intent. No postoperative complication was recorded. Nine patients received postoperative chemotherapy. None received preoperative chemotherapy. The pathologic stages were I in 7, II in 6, and III in 4 cases. Follow-up data were available for all patients with duration of 1 to 85 months (median, 29.3 mo). Six patients developed distant metastases (case 1, adrenal; case 5, adrenal and bone; case 6, brain; case 10, brain and adrenal; case 11, lung; case 12, liver), and an additional patient had a metastasis to hilar lymph nodes (case 14) after surgery. Three-year and 5-year disease-free survival rates were 48.6% and 48.6%, respectively, and 3-year and 5-year overall survival rates were 71.4% and 53.6%, respectively.

Histopathologic Findings

The histologic characteristics of HG-LAFMs are presented in Table 3 and are shown in Figure 1. The tumors measured 1.9 to 9.5 cm (average, 5.0 cm). All the

TABLE 2. *EGFR* and *KRAS* High-Resolution Melting Analysis Primer Sequences

Exon	Primer Name	Sequence	Amplicon Size
21 (L858R)	*EGFR*_ex18_F	5′-AGATCACAGATTTTGGGC-3′	51 bp
	*EGFR*_ex18_R	5′-ATTCTTTCTCTTCCGCAC-3′	
19 (deletion)	*EGFR*_ex19_F	5′-AAAATTCCCGTCGCTATC-′3	83 bp
	*EGFR*_ex19_R	5′-AAGCAGAAACTCACATCG-′3	
2 (189 bp)	*KRAS* (codon12, 13, 189 bp)_ex2_F	5′-TCATTATTTTTATTATAAGGCCTGCTGAA-3′	189 bp
	KRAS (codon12, 13, 189 bp)_ex2_R	5′-CAAAGACTGGTCCTGCACCAGTA-3′	
2 (92 bp)	*KRAS* (codon12, 13, 92 bp)_ex2_F	5′-TTATAAGGCCTGCTGAAAATGACTGAA-3′	92 bp
	KRAS (codon12, 13, 92 bp)_ex2_R	5′-TGAATTAGCTGTATCGTCAAGGCACT-3′	
2 (62 bp)	*KRAS* (codon12, 13, 62 bp)_ex2_F	5′-TAAACTTGTGGTAGTTGGAGC-3′	62 bp
	KRAS (codon12, 13, 62 bp)_ex2_R	5′-GAATTAGCTGTATCGTCAAGG-3′	
3 (codon 61)	*KRAS* (codon61)_ex3_F	5′-CACTGTAATAATCCAGACTGTGTTTC-3′	266 bp
	KRAS (codon61)_ex3_R	5′-AACTATAATTACTCCTTAATGTCAGCTT-3′	

TABLE 3. Clinical and Histopathologic Features of 17 High-grade Lung Adenocarcinomas with Fetal Lung–like Morphology

Case	Age (y)	Sex	Smoking (p-y)	Size (cm)	Stage	Histologic Patterns: Fetal (%)	Hep (%)	Clear (%)	LCNEC (%)	Others (%)	Histology in LN Metastasis	Follow-up (mo)
1	61	M	91	8.0	IIIA	60	—	15	—	Aci 20, pap 5	Aci, pap, fetal	DOD (55)
2	70	M	37.5	1.9	IA	50	—	—	—	Lep 30, pap 10, aci 10	—	NED (85)
3	67	M	47	5.0	IB	20	10	20	45	Pap 5	—	NED (61)
4	69	M	37	3.8	IB	30	—	35	10	Pap 10, aci 10, lep 5	—	NED (48)
5	73	M	55	5.5	IB	5	—	—	—	Aci 65, pap 15, lep 10, sol 5	—	AWD (15)
6	65	M	45	4.5	IIB	20	—	20	20	Aci 20, pap 10, lep 10	LCNEC	DOD (26)
7	58	M	114	3.5	IIB	15	30	45	—	Aci 10	—	NED (13)
8	53	M	45	7.3	IIB	5	5	10	60	Aci 20	—	NED (12)
9	62	F	21	5.5	IB	10	40	10	—	Aci 10, pap 10, sol 20	—	NED (12)
10	40	M	50	6.5	IIIA	30	—	25	—	Pap 20, aci 15, sol 10	Aci, fetal	AWD (24)
11	65	M	NA	6.5	IIIA	15	—	15	—	Aci 40, pap 20, sol 10	Fetal, clear, pap	DOD (21)
12	69	M	49	4.5	IIB	30	—	60	—	Pap 10	Pap	DOD (9)
13	55	M	28	4.0	IIIB	20	—	20	—	Aci 40, pap 10, sol 5, lep 5	—	NED (26)
14	74	M	100	3.0	IIB	5	25	50	—	Sol 10, aci 10	Sol, fetal, clear	AWD (12)
15	73	M	40	9.5	IB	30	—	15	—	Aci 20, lep 20, pap 10, sol 5	—	NED (18)
16	75	M	NA	3.2	IB	45	—	15	—	Pap 40	—	NED (60)
17	62	M	63	3.5	IIB	40	—	20	—	Pap 20, aci 15, sol 5	—	NED (1)

Aci indicates acinar pattern; AWD, alive with disease; clear, clear-cell; DOD, died of disease; F, female; fetal, fetal lung–like; hep, hepatoid; lep, lepidic pattern; LN, lymph node, M, male; NA, data not available; NED, no evidence of disease; pap, papillary pattern; sol, solid pattern.

17 tumors showed at least focal area resembling fetal lung epithelium by selection criteria (Figs. 1A, B). The fetal lung–like component accounted for 5% to 60% (average, 25%) of the total tumor volume. None of the 17 tumors consisted entirely of fetal lung–like morphology. No tumor showed morule formation. The coexisting non–fetal lung–like components consisted of conventional adenocarcinoma that displayed various patterns including lepidic (6 cases, 35%), papillary (14 cases, 82%), acinar (14 cases, 82%), and solid (8 cases, 47%) patterns (Fig. 1C). In addition to such conventional patterns, a hepatoid pattern was identified in 5 cases (29%, Fig. 1D) and clear-cell component (exclusive of fetal lung–like element) was observed in 15 cases (88%; Fig. 1E). Four cases had a large cell neuroendocrine carcinoma (LCNEC) component (cases 3, 4, 6, and 8; Fig. 1F). None of the 17 cases harbored squamous cell or small cell differentiation. None was a biphasic tumor with sarcomatoid element. Lymphovascular and pleural invasions were identified in 14 and 11 cases, respectively. Necrosis was identified in all cases, and 13 cases (76%) showed grossly visible massive necrosis. Lymph node metastasis was identified in 6 cases (35%), of which 4 lesions showed fetal lung–like morphology.

Immunohistochemical Findings

Immunostaining results are presented in Figures 2 and 3. Both fetal lung–like and coexisting non–fetal lung–like components were often positive for oncofetal proteins such as AFP (Fig. 3A), GPC-3 (Fig. 3B), and SALL-4 (Fig. 3C). These oncofetal proteins were more frequently positive in the non–fetal lung–like component, particularly in the clear-cell and hepatoid patterns, than in the fetal lung–like component. Specifically, the fetal lung–like component was positive for AFP, GPC-3, and SALL-4 in 29%, 76%, and 53%, respectively, whereas the non–fetal lung–like component labeled for these markers in 41%, 88%, and 59%, respectively. Similarly, at least 1 of 3 neuroendocrine markers (ie, synaptophysin, chromogranin A, and neural cell adhesion molecule) was positive in most (82%) cases, and it was more frequently positive in the non–fetal lung–like component (82%) than in the fetal lung–like component (65%) (Fig. 3D). Thyroid transcription factor-1, CDX-2, and p53 were positive in 41%, 35%, and 59% of fetal lung–like components, respectively; they were positive in 53%, 35%, and 65% of non–fetal lung–like component, respectively (Figs. 3E, F). No nuclear or cytoplasmic aberrant expression of β-catenin was observed in any of the 17 cases.

Molecular Characteristics

Molecular characteristics of HG-LAFMs are presented in Table 4. Mutation analyses of *EGFR* and *KRAS* genes were performed in 14 and 9 cases, respectively. One case harbored L858R mutation of *EGFR*, and another showed *KRAS* mutation in either codon 12 or 13. The remaining cases tested were of wild type for both *EGFR* and *KRAS*.

DISCUSSION

This comprehensive study of HG-LAFMs clarified their clinicopathologic characteristics and highlighted its difference from the reported traits of low-grade adenocarcinoma of fetal lung type.[8,11] In addition to an unfavorable prognosis inherently attached to high tumor grade, the differences include the following. First,